How does the Southern Ocean palaeoenvironment during Marine Isotope Stage 5e compare to the modern?

M. Chadwick[1,2*]; C.S. Allen[1]; L.C. Sime[1]; X. Crosta[3] & C.-D. Hillenbrand[1]

[1.] British Antarctic Survey, High Cross, Madingley Road, Cambridge, CB3 0ET, UK

[2.] Ocean and Earth Science, National Oceanography Centre, University of Southampton Waterfront Campus, European Way, Southampton, SO14 3ZH, UK

[3.] Université de Bordeaux, CNRS, EPHE, UMR 5805 EPOC, Pessac, France

**Corresponding author:* machad27@bas.ac.uk, British Antarctic Survey, High Cross, Madingley Road, Cambridge, UK

Abstract

Marine Isotope Stage (MIS) 5e (130-116 ka) represents an important 'process analogue' for understanding the climatic feedbacks and responses likely active under future anthropogenic warming. Reconstructing the Southern Ocean (SO) palaeoenvironment during MIS 5e and comparing it to the present day provides insights into the different responses of the SO sectors to a warmer climate. This study presents new records from seven marine sediment cores for MIS 5e together with their surface sediment records; all cores are located south of 55 ^{o}S. We investigate changes in diatom species assemblage and the accompanying variations in sea surface temperatures, winter sea-ice extent (WSIE) and glacial meltwater flux. All records show warmer conditions and a reduced WSIE during MIS 5e relative to the surface sediments. While the Pacific and Indian Sector records present very stable conditions throughout MIS 5e, the Atlantic Sector records display much more changeable conditions, particularly with respect to the WSIE. These variable conditions are attributed to higher iceberg and glacial meltwater flux in the Weddell Sea. This evidence for increased iceberg and glacial meltwater flux in the Weddell Sea during MIS 5e may have significant implications for understanding the stability of the West Antarctic Ice Sheet, both during MIS 5e and under future warming.

Keywords

MIS 5e; Palaeoenvironment; Diatom; Southern Ocean; Marine Sediment Core

1. Introduction

The Antarctic continent and Southern Ocean (SO) play a critical role in the global climate system through the albedo-radiation feedbacks induced by the vast extent of the Antarctic ice sheets and SO sea ice. Sea-ice cover also regulates heat and gas exchange between the SO and the atmosphere and, through changes in sea surface temperatures (SSTs) and salinity, affects Antarctic Bottom Water production and thereby impacts upon global ocean circulation (Abernathey et al. 2016).

Rising greenhouse gas concentrations are driving current global warming, with polar regions warming twice as fast as the global average (IPCC 2019). High latitudes have a greater sensitivity to radiative forcing and therefore tend to amplify the effects of rising temperatures through ocean and cryosphere feedbacks (Vaughan et al. 2013). This greater sensitivity makes higher latitudes particularly important regions for studying and understanding climate dynamics. However, the very short length of observational records limits our understanding of the underlying processes. Studying past warm periods, when the extent of land ice and sea ice were reduced, can help guide our understanding of the impact of predicted future climate change in these key regions.

Marine Isotope Stage (MIS) 5e (130 – 116 ka) was the last period when the Antarctic region was substantially warmer. SSTs and global mean annual atmospheric temperatures peaked at around 0.8 ^{o}C warmer during MIS 5e than present (Otto-Bliesner et al. 2013, Capron et al. 2014, Fischer et al. 2018) and global sea levels were possibly 5-9 m higher than now (Kopp et al. 2009). Proxy reconstructions of mean annual SSTs in middle to low latitudes (between 51 ^{o}N and 51 ^{o}S) peaked at just 0.5 ± 0.3 ^{o}C warmer than preindustrial during MIS 5e (Hoffman et al. 2017) whereas model results suggest that summer SSTs in the SO peaked at 1.8 ± 0.8 ^{o}C warmer than preindustrial (Capron et al. 2017), indicating strong polar amplification during MIS 5e. Unlike future anthropogenic warming, MIS 5e peak temperatures were orbitally forced rather than primarily through rising greenhouse gas concentrations, making MIS 5e an important 'process analogue' for understanding the climate mechanisms and natural feedbacks that will be active under future warmer conditions (Stone et al. 2016).

In the modern SO there is substantial spatial heterogeneity in the observed sea-ice trends, with sea-ice reductions in the Bellingshausen and Amundsen seas concurrent with increases in the (outer) Weddell Sea and Ross Sea Sectors (Stammerjohn et al. 2008a, Hobbs et al. 2016, Parkinson 2019). Trends in modern SO surface, deep and bottom water temperatures display similar heterogeneity (Maheshwari et al. 2013, Schmidtko et al. 2014). Model simulations are unable to replicate the observations of recent sea-ice change without reducing the regional warming trends (Rosenblum & Eisenman 2017). These difficulties are indicative of the complexities of the climate dynamics, which drive SST and sea-ice change in the SO today (Stammerjohn et al. 2008b, King 2014, Hobbs et al. 2016, Purich et al. 2016). Model deficiencies in the SO region suggest that the large signal-to-noise ratio in SO temperature and sea-ice conditions during MIS 5e will be useful for improving climate model simulations of this region for warmer climates.

The diatom assemblages preserved in SO marine sediments are a valuable tool for reconstructing past oceanographic conditions. Diatoms are phototrophic algae, which are prevalent in the SO euphotic zone, and their species distribution patterns are closely related to the environmental conditions in the surface waters, principally the sea ice cover and SSTs (Zielinski & Gersonde 1997, Gersonde & Zielinski 2000, Armand et al. 2005, Crosta et al. 2005, Romero et al. 2005, Esper et al. 2010). Several previous studies have used marine sediment core records to reconstruct the palaeoceanographic conditions during MIS 5e, often alongside model simulations (Bianchi & Gersonde 2002, Turney & Jones 2010, Otto-Bliesner et al. 2013, Capron et al. 2014, Hoffman et al. 2017, Turney et al. 2020). However, these studies contain few, or no, marine records from south of 55 ^{o}S and therefore are unable to capture the MIS 5e environmental conditions in the Antarctic Zone (south of the Polar Front). Due to the uncertainties in the chronologies of SO proxy records (Govin et al. 2015), previous studies have often either averaged SSTs across MIS 5e (Cortese et al. 2013, Turney et al. 2020) or assumed peak SSTs occur synchronously throughout the SO and are coincident with peak atmospheric temperatures in Antarctica (Otto-Bliesner et al. 2013, Capron et al. 2014, Hoffman et al. 2017).

This study aims to compare the environmental conditions in the SO between MIS 5e and the modern using diatom assemblage data preserved in marine sediments. New MIS 5e assemblage data from seven sediment cores located south of 55 ^{o}S (Figure 1) are compared to the surface sediment assemblages to determine whether all three sectors of the SO had warmer SSTs and a reduced winter sea-ice extent (WSIE) during MIS 5e, relative to the modern, and whether changes in SSTs and WSIE during MIS 5e occurred in a uniform pattern across all SO sectors.

2. Modern oceanography

The SO comprises the southern-most basins of the Atlantic, Indian and Pacific oceans and acts as a linkage between the water masses and oceanic circulation within these basins. The dominant oceanographic feature in the modern SO is the clockwise flowing Antarctic Circumpolar Current (ACC), which forms a continuous belt separating subtropical waters to the north from Antarctic waters to the south (Orsi et al. 1995). The ACC is characterised by five fronts, marked by steep horizontal density gradients associated with specific SSTs and salinities (Orsi et al. 1995, Dong et al. 2006, Sokolov & Rintoul 2009). The most southerly fronts are the Southern Boundary of the ACC and the Southern ACC Front (Orsi et al. 1995), which do not separate distinct surface water masses and thus will not be considered in this study. The Subtropical Front marks the northern boundary of the ACC, separating Subantarctic and Subtropical surface waters, and is located too far north (~40 ^{o}S) to influence the core sites used in this study. The Subantarctic Front is the most northerly of the remaining two fronts (white line in Figure 1) and is marked by SSTs ≥8 ^{o}C to the north and SSTs ≤7 ^{o}C to the south (Meinen et al. 2003). The final ACC front is the Polar Front (black line in Figure 1) which is marked by the subsurface (200 m) 2 ^{o}C isotherm (Orsi et al. 1995) and generally corresponds to SSTs of ~2-3 ^{o}C (Dong et al. 2006).

The Subantarctic Front separates the Subantarctic Zone (to the north) from the Polar Front Zone (to the south), which is in turn separated from the more southerly Antarctic Zone by the Polar Front (Orsi et al. 1995).

The flow of deep and bottom water masses and the locations of the ACC fronts are strongly influenced by the SO bathymetry. Bathymetric highs, such as the Kerguelen Plateau and Pacific-Antarctic Ridge, and oceanic gateways, such as the Drake Passage and Tasman Gateway, act to 'pin' and constrain ACC fronts and restrict their latitudinal migration (Dong et al. 2006).

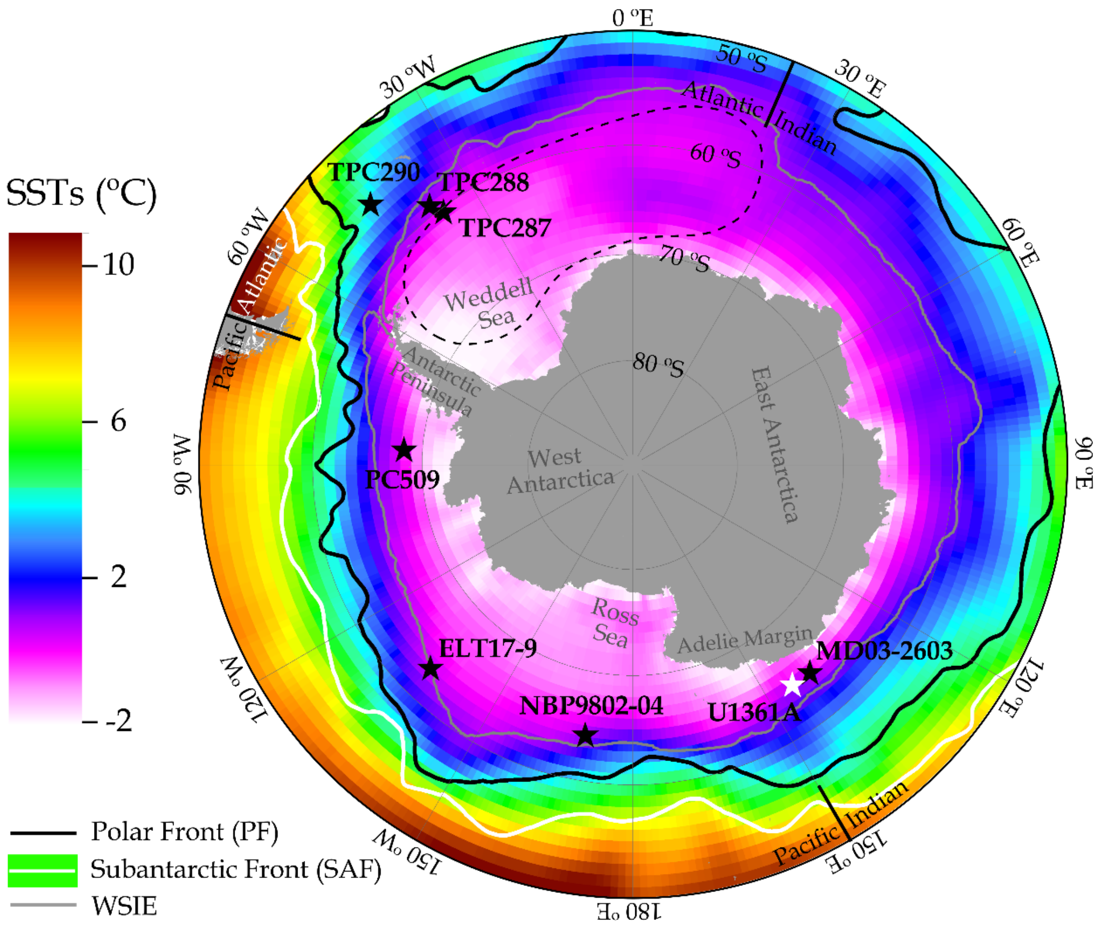

Figure 1: Map of core locations (black stars) with modern SSTs, locations of SO fronts and WSIE. The white star indicates a surface sediment sample (U1361A) assumed to contain a modern diatom assemblage characteristic for the Indian Sector. The white line marks the modern Subantarctic Front (position from Orsi et al. (1995)), the solid black line marks the modern Polar Front (position from Trathan et al. (2000)), the dashed black line marks the extent of the Weddell Gyre (Vernet et al. 2019) and the grey line marks the mean September sea-ice extent from 1981-2010 (data from Fetterer et al. (2017)). The background shadings display the mean annual SSTs from 1981-2010 using the COBE-SST2 dataset provided by the NOAA PSL, Boulder, Colorado, USA (https://psl.noaa.gov/). The boundaries between the three SO sectors (Atlantic, Indian and Pacific) are highlighted by straight black lines.

3. Materials and methods

3.1. Core sites

This study presents new MIS 5e diatom assemblage data from seven marine sediment cores (Table 1 & Figure 1) in all sectors of the SO – three in the Atlantic Sector (70 °W – 20 °E), one in the Indian Sector (20 °E – 150 °E) and three in the Pacific Sector (150 °E – 70 °W). These cores were selected as they contain >20 cm thick intervals of diatom rich MIS 5e sediments and are located further south than almost all cores with existing MIS 5e diatom records (Chadwick et al. 2020). Seafloor surface sediment from an additional Indian Sector core, International Ocean Discovery Program (IODP) Expedition 318 Hole U1361A, is also included.

Core	Latitude, Longitude	Water depth (m)	Cruise, Year	Ship	Core length (cm)
TPC290	55.55 °S, 45.02 °W	3826	JR48, 2000	*RRS James Clark Ross*	1179*
TPC288	59.14 °S, 37.96 °W	2864	JR48, 2000	*RRS James Clark Ross*	940*
TPC287	60.31 °S, 36.65 °W	1998	JR48, 2000	*RRS James Clark Ross*	615*
ELT17-9	63.08 °S, 135.12 °W	4935	ELT17, 1965	*R/V Eltanin*	2018
NBP9802-04	64.20 °S, 170.08 °W	2696	PA9802, 1998	*RV/IB Nathaniel B. Palmer*	740
MD03-2603	64.28 °S, 139.38 °E	3320	MD130, 2003	*R/V Marion DuFresne II*	3033
U1361A	64.41 °S, 143.89 °E	3459	IODP Exp. 318, 2010	*JOIDES Resolution*	38800
PC509	68.31 °S, 86.03 °W	3559	JR179, 2008	*RRS James Clark Ross*	989

Table 1: Details of the location and recovery information for the eight sediment cores analysed in this study. Cores are ordered by latitude. For IODP Site U1361*,* only the core top surface sample from Hole U1361A was analysed. *For the three TPC cores (TPC290, TPC288 and TPC287), a trigger core and piston core were taken at the same location, and the records were spliced together to form a composite trigger-piston core record.

3.2. Diatom counts

For the diatom assemblage data, microscope slides were produced using a method adapted from Scherer (1994). Samples of 7-20 mg were exposed to 10% hydrochloric acid to remove any carbonate, 30% hydrogen peroxide to break down organic material and a 4% sodium hexametaphosphate solution to promote disaggregation during their placement in a warm water bath for a minimum of 12 hours. The material was homogenised into a ~10 cm water column and allowed to settle randomly onto coverslips over a minimum of 4 hours. The water was drained away and coverslips were mounted on microscope slides with Norland Optical Adhesive (NOA 61). Slides were investigated with a light microscope (Olympus BH-2 at x1000 magnification) and a minimum of 300 diatom valves were counted for each sample.

Diatom species/genera	Modern summer SST (°C)	Modern sea-ice duration (months/yr)
Actinocyclus actinochilus	-0.5 – 0.5 [a]	7.5 - 9 [a]
Azpeitia tabularis	1 – 22.5 [b]	0 – 3.5 [b]
Chaetoceros rs.	-1.3 – 3.5 [a]	0 – 10.5 [a]
Eucampia antarctica	-2 – 9.5 [c]	–
Fragilariopsis curta	-1.3 – 2.5 [a]	5 – 10.5 [a]
Fragilariopsis cylindrus	-1.3 – 1 [a]	7.5 – 10.5 [a]
Fragilariopsis kerguelensis	-1 – 22 [d]	0 – 9 [d]
Rhizosolenia antennata f. *semispina*	0.5 – 2 [e]	1 – 3.5 [d]

Table 2: Modern summer SSTs and sea-ice duration ranges for diatom species and genera that are presented in this study. The SST and sea-ice duration ranges for the present day are based on surface samples where the listed species/genera is >2 % of the assemblage. *Eucampia antarctica* does not show any clear association with modern sea-ice duration. [a] Armand et al. (2005), [b] Romero et al. (2005), [c] Zielinski & Gersonde (1997), [d] Crosta et al. (2005), [e] Armand & Zielinski (2001).

Diatom relative abundances for each sediment core are reported for species or groups with well-constrained present-day ecologies/habitats (Table 2). *Actinocyclus actinochilus* is a cold-water species (Table 2) generally found in low abundances (<3 %) in SO seafloor surface sediment samples within the maximum WSIE (Armand et al. 2005, Esper & Gersonde 2014b). Increasing relative abundances of this species in southern high latitude sediments suggest colder SSTs and more severe sea-ice cover. *Azpeitia tabularis* is a warm-water species (Table 2), reaching up to 20 % of the total diatom assemblages in the Subantarctic Zone and presenting relative abundances <5 % in surface sediments south of the Polar Front (Romero et al. 2005, Esper & Gersonde 2014b). This species additionally has a southerly occurrence restricted by the maximum WSIE (Zielinski & Gersonde 1997). Increasing abundances of this group in southern high latitude sediments therefore suggest warmer SSTs and ice-free conditions.

The abundance of *Chaetoceros* rs. in SO surface sediments is dominantly influenced by meltwater surface stratification and nutrient availability (Armand et al. 2005), with high surface stratification and nutrient availability resulting in *Chaetoceros* rs. dominated assemblages (>60 %) in coastal Antarctic systems (Leventer & Dunbar 1988, Leventer 1991, 1992, Crosta et al. 1997). High *Chaetoceros* rs. abundances are also associated with moderately consolidated winter sea ice (sea-ice duration = 3-9 months/yr), but this relationship is still poorly understood (Armand et al. 2005). The *Chaetoceros* rs. abundances in this study include a small number (up to 1 %) of *Chaetoceros* (*Hyalochaete*) vegetative cells in some samples. Other than *Chaetoceros* rs., *Fragilariopsis kerguelensis* is the dominant diatom species/group in SO surface sediments, with the greatest abundances found in locations with year-round open ocean conditions (Crosta et al. 2005, Cefarelli et al. 2010, Esper et al. 2010) and, as a result, changes in *F. kerguelensis* abundance are often negatively correlated with changes in *Chaetoceros* rs. abundance. Taken together, an increase in the relative abundance of *F. kerguelensis*, and concurrent decrease in the relative abundance of *Chaetoceros* rs. in our core records indicate a shift from conditions with moderate sea-ice cover and stratified surface waters to open ocean conditions with low or no winter sea-ice cover.

Fragilariopsis curta and *F. cylindrus*, composing the FCC group, are sea-ice associated species (Kang & Fryxell 1992, Beans et al. 2008), presenting their maximum abundances in modern sediments at winter sea-ice concentrations >70 % and SSTs <1 °C (Armand et al. 2005, Esper & Gersonde 2014b, a). The FCC group is used as an indicator of winter sea-ice presence (Gersonde & Zielinski 2000), with abundances >3 % associated with locations south of the mean WSIE, abundances 1-3 % found between the mean and maximum WSIE and abundances <1 % being indicative of conditions north of the maximum WSIE (Gersonde & Zielinski 2000, Gersonde et al. 2005). Increasing relative abundances of the FCC group in our cores therefore infer heavy sea-ice conditions and cold SSTs.

The abundance of *Eucampia antarctica* in SO surface sediments does not show a clear pattern relative to SSTs or sea-ice extent (Zielinski & Gersonde 1997), probably because its two varieties have usually been combined in abundance counts. The cold variety of *E. antarctica* has, however, been related to iceberg flux, with high iceberg flux promoting high *E. antarctica* abundances through meltwater-induced buoyancy and high iron availability (Burckle 1984, Fryxell & Prasad 1990, Allen 2014). Based on restricted modern studies, high relative abundances of *E. antarctica* cold variety encountered downcore have been used as an indicator of iceberg or marine-terminating glaciers melting (Barbara et al. 2016). The *E. antarctica* relative abundances reported in this study only include valves from the cold variety. *Rhizosolenia antennata* f. *semispina* reaches its maximum abundance in SO surface sediments located within, and just north of, the mean WSIE (Crosta et al. 2005) and is also an indicator of high meltwater flux and surface stratification (Allen et al. 2005).

Surface sediment samples from four of the core sites (TPC290, TPC288, TPC287 and PC509) are used to obtain modern diatom assemblages for those sites. For core MD03-2603, the surface sediment sample from the nearby Site U1361 (Table 1 & Figure 1) is used for the modern diatom assemblage. There was no surface material available for the central Pacific Sector cores (ELT17-9 and NBP9802-04), so the MIS 5e diatom assemblages in these cores are not compared against any modern assemblages. Using surface sediment samples to represent the modern surface water conditions is consistent with previous studies (Zielinski & Gersonde 1997, Crosta et al. 1998, Armand et al. 2005, Crosta et al. 2005, Romero et al. 2005, Esper & Gersonde 2014b, a), but we note that the assemblage preserved in surface sediments is likely an integrated signal of up to 500 years (Miklasz & Denny 2010).

4. Age models

4.1. Published chronologies

Of the seven sediment cores, for which MIS 5e data are presented in this study, five utilise previously published age models (Table 3). The chronology for cores TPC290 and TPC288 is given in Pugh et al. (2009) and utilises the correlation between the magnetic susceptibility (MS) record in marine sediment cores from the Scotia Sea and the dust record in the EPICA Dome C (EDC) ice core over past glacial-interglacial cycles (Pugh et al. 2009, Weber et al. 2012). In both cores this chronology is combined with the abundance stratigraphy of the radiolarian species *Cycladophora davisiana*, with the e_3 low abundance event indicating MIS 5e (Brathauer et al. 2001). The Termination II tiepoint in TPC290 was adjusted from the 7.11 metres below seafloor (mbsf) given in Pugh et al. (2009) to 7.23

Core	Latitude, Longitude	SO sector	Chronology for MIS 5e	MIS 5e sampling interval (ka)
TPC290	55.55 °S, 45.02 °W	Atlantic	Correlating MS from TPC290 to EDC ice core dust record combined with *C. davisiana* abundances (Pugh et al. 2009)*	0.6
TPC288	59.14 °S, 37.96 °W	Atlantic	Correlating MS from TPC288 to EDC ice core dust record combined with *C. davisiana* abundances (Pugh et al. 2009)	0.7 - 1.1
TPC287	60.31 °S, 36.65 °W	Atlantic	Correlating MS from TPC287 to MS from TPC288 (this study; Figure 2)	0.5 - 1.2
ELT17-9	63.08 °S, 135.12 °W	Pacific	Combined abundance stratigraphies of *E. antarctica* and *C. davisiana* on SPECMAP age scale (Chase et al. 2003)	1.2 - 1.3
NBP9802-04	64.20 °S, 170.08 °W	Pacific	Correlating MS from NBP9802-04 to EDC ice core dust record combined with Last Occurrence Datum of *H. karstenii* (Williams 2018)	1.4
MD03-2603	64.28 °S, 139.38 °E	Indian	Correlating Ba/Al and Ba/Ti ratios from MD03-2603 to LR04 benthic oxygen isotope stack combined with diatom biostratigraphy (Presti et al. 2011)	0.4 - 0.9
PC509	68.32 °S, 86.03 °W	Pacific	Correlating wet bulk density (=proxy mirroring biogenic opal content) from PC509 to the LR04 benthic oxygen isotope stack (this study; Figure 3)	0.6 - 1.3

Table 3: Summary of the locations and chronologies for the seven sediment cores analysed in this study. Cores are ordered by latitude. *For core TPC290 the chronology was adjusted from the age model previously published in Pugh et al. (2009) by shifting the Termination II tiepoint to improve alignment of its MS signal with the EDC dust record.

mbsf to improve the alignment of the MS signal of the sediments with the EDC dust record. The chronology for core NBP9802-04 also utilises the correlation between sediment MS and EDC dust (Pugh et al. 2009), alongside the presence/absence of the diatom species *Hemidiscus karstenii* (Williams 2018), which is a biostratigraphic marker for the MIS 6/7 boundary (Burckle et al. 1978). All three of these cores have chronologies tied to the EDC3 time scale (Parrenin et al. 2007).

Cores MD03-2603 and ELT17-9 have published chronologies tied to the LR04 and SPECMAP age scales, respectively (Table 3). For core MD03-2603, Presti et al. (2011) correlated the downcore records of Ba/Al and Ba/Ti ratios, which are palaeo-productivity proxies, to the LR04 benthic foraminifera $\delta^{18}O$ stack (Lisiecki & Raymo 2005). The chronology for core ELT17-9 was published by Chase et al. (2003) and uses abundances for *C. davisiana* (Hays J. unpublished data) and *E. antarctica* (Burckle L.H. unpublished data), which provide well established abundance stratigraphies (Burckle & Burak 1995, Brathauer et al. 2001). To allow for consistent comparison of timings between cores, both MD03-2603 and ELT17-9 are translated across onto the EDC3 chronology using the conversion tables published by Lisiecki & Raymo (2005) and Parrenin et al. (2013). During MIS 5e, EDC3 ages are ~1 ka older than LR04 ages, with this offset due to the LR04 chronology being based upon a benthic record that incorporates both sea-level and temperature components (Parrenin et al. 2007). A chronology tuned to surface water rather than deep water changes was chosen because we are investigating environmental changes in the surface ocean.

4.2. *TPC287 chronology*

The chronology for core TPC287 was constructed by aligning the downcore MS records in cores TPC287 and TPC288 (Figure 2). TPC287 is located approximately 150 km southeast of TPC288 (Figure 1), and thus the MS variations in both cores are expected to occur synchronously across glacial and interglacial cycles. The two MS records were graphically aligned by eye using the AnalySeries software (Paillard et al. 1996) by choosing prominent features as tiepoints (Figure 2 & Table 4).

4.3. *PC509 chronology*

The chronology for core PC509 was constructed by visually aligning the wet bulk density, a proxy mirroring biogenic opal content (Busch 1991, Weber et al. 1997, Hillenbrand et al. 2009), to the LR04 benthic foraminifera $\delta^{18}O$ stack (Lisiecki & Raymo 2005) using the AnalySeries software (Paillard et al. 1996). Tiepoints were selected in the wet bulk density record at MIS stage and sub-stage boundaries (Table 5 & Figure 3). The MIS 5 sub-stages use the age assignments from Govin et al. (2009), and the ages are translated across from the LR04 chronology to the EDC3 chronology using the conversion table published by Parrenin et al. (2013).

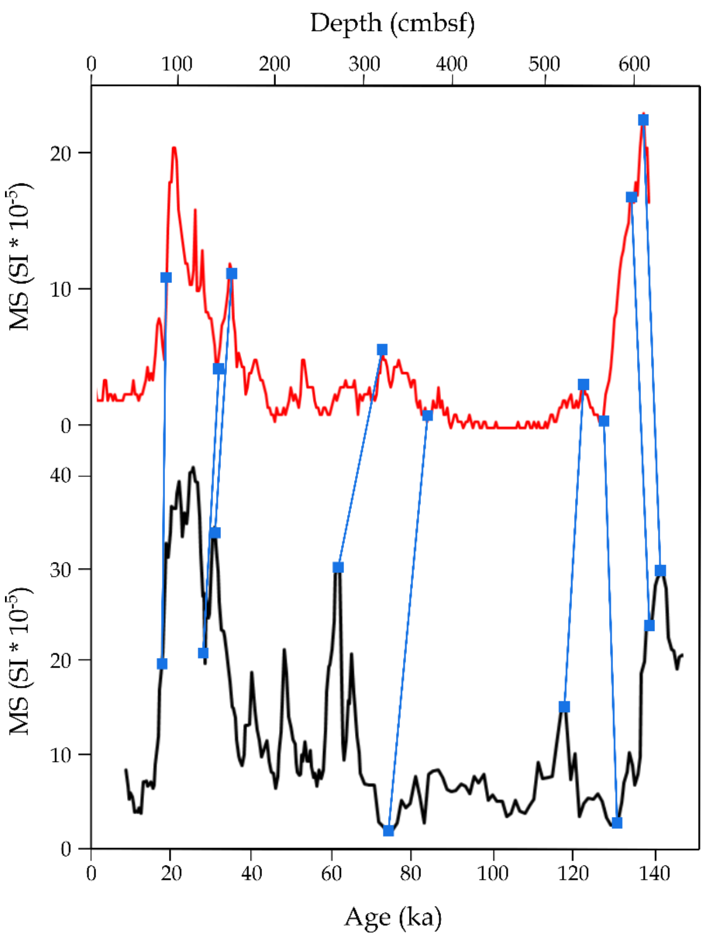

Figure 2: Alignment between the MS downcore records from cores TPC287 (red) and TPC288 (black) using the AnalySeries software (Paillard et al. 1996). The blue squares and connecting lines mark tiepoints between the records. The age model for core TPC288 was published by Pugh et al. (2009).

TPC287 depth (mbsf)	TPC288 age (ka)
0.84	17.5
1.39	28.5
1.53	31
3.21	61
3.71	74
5.43	118
5.65	131
5.95	138.5
6.09	142

Table 4: Tiepoints for the TPC287 chronology with depths in core TPC287 being tied to the EDC3 ages published by Pugh et al. (2009) for core TPC288.

PC509 depth (mbsf)	LR04 age (ka)	MIS stage/sub-stage boundary
5.00	73	4-5a
5.20	84	5a-5b
5.64	91	5b-5c
5.78	106	5c-5d
5.97	116	5d-5e
6.38	130	5e-6
6.48	136	-

Table 5: Tiepoints for the PC509 chronology. The wet bulk density record for PC509 was aligned with the LR04 benthic stack using the AnalySeries software (Paillard et al. 1996). The ages for MIS stage/sub-stage boundaries used as tiepoints are listed.

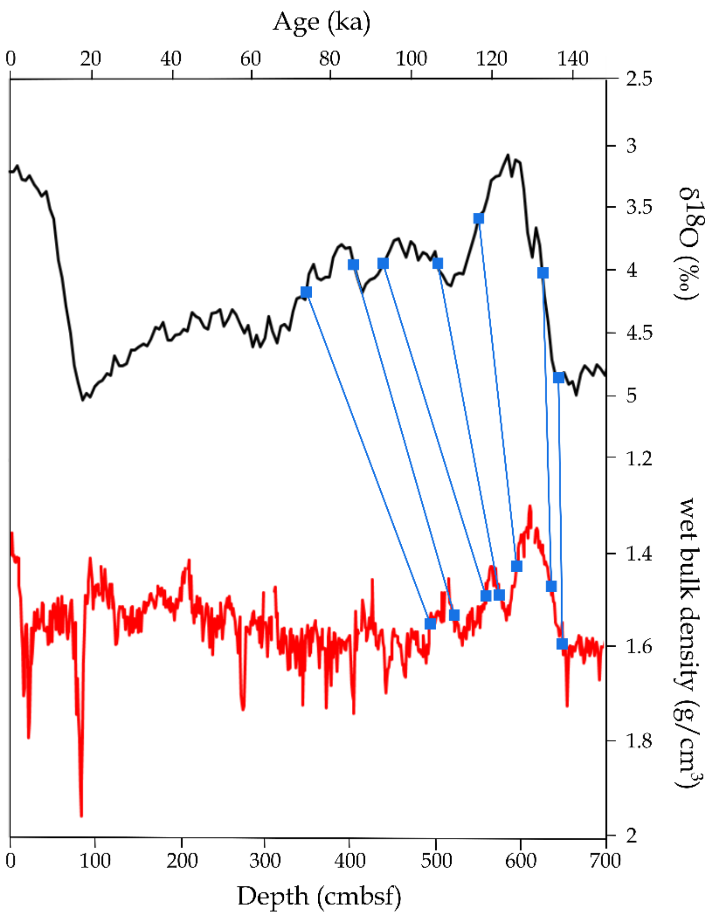

Figure 3: Alignment between the downcore wet bulk density record of core PC509 (red) and the LR04 benthic δ^{18}O stack (black) using the AnalySeries software (Paillard et al. 1996). The tiepoints are marked by blue squares and connecting lines.

5. Results and discussion

5.1. *MIS 5e diatom assemblages*

Relative diatom abundances in the sediments deposited during the time interval 132-120 ka are presented for all seven core sites (Figures 4-6) in order to capture the palaeoenvironmental signal both from the Termination II deglaciation and 'peak' MIS 5e. The *Azpeitia tabularis* and *Actinocyclus actinochilus* abundances are low in all seven cores (0.3 ± 0.4 % and 0.5 ± 0.6 %), with cores TPC288, ELT17-9 and PC509 recording only negligible contributions (0.3 ± 0.3 %) of either species (Figures 4-6). Core TPC287 has the largest 'cold signal' (Table 2), with an *A. actinochilus* peak of 2 % at 120 ka (Figure 4), and core TPC290 has the greatest 'warm signal' (Table 2) with high *A. tabularis* abundances of 1.8 ± 0.7 % and 2.0 ± 0.4 % from 126-124 ka and 121-120 ka, respectively (Figure 4). Core NBP9802-04 also has a strong 'warm signal' with *A. tabularis* being present almost throughout MIS 5e (Figure 6).

The highest MIS 5e *Chaetoceros* rs. abundances occur in core PC509 (78 ± 4 %). This is likely due to high input of meltwater and nutrients, like in the vicinity of the Antarctic Peninsula, where high meltwater stratification and nutrient availability promote extensive *Chaetoceros* blooms (Crosta et al. 1997). The three Atlantic Sector cores (TPC290, TPC288 and TPC287) are dominated by both *Chaetoceros* rs. (38 ± 10 %, 40 ± 8 % and 28 ± 11 %, respectively) and *F. kerguelensis* (34 ± 8 %, 27 ± 6 % and 33 ± 12 %, respectively) throughout MIS 5e with peaks in one group coinciding with troughs in the other (Figure 4). This alternation is particularly evident in core TPC287, where *Chaetoceros* rs. abundance declined by ~40 % after 131 ka, concurrent with an equivalent increase in *F. kerguelensis* abundance (Figure 4). Both TPC288 and TPC287 have similar *F. kerguelensis* abundance profiles with higher values of 34 ± 4 % and 53 ± 6 %, respectively, between 130-127 ka and 126-124 ka (Figure 4). This contrasts with core TPC290, where the *F. kerguelensis* abundance is lowest (27 ± 4 %) from 128-122 ka (Figure 4). Consistent with the modern distribution pattern published by Crosta et al. (1997), the Indian and central Pacific Sector cores (ELT17-9, NBP9802-04 and MD03-2603) have low *Chaetoceros* rs. abundances (10 ± 2 %, 5 ± 2 % and 17 ± 5 %, respectively) during MIS 5e and are dominated instead by *F. kerguelensis* (63 ± 4 %, 74 ± 4 % and 59 ± 8 %, respectively) (Figures 5 & 6).

The FCC abundances in cores TPC288 and TPC287 are very similar with minima (0.3 % and 1 %) early in the 132-120 ka interval, followed by an increase to maxima of ~9 % and ~15 %, respectively, at ~127-126 ka before decreasing to largely steady abundances of ~3 % and ~6 %, respectively, between 125 and 120 ka (Figure 4). In contrast, the FCC abundances in core TPC290 remain largely consistent at 2.3 ± 0.7 % from 130 to 124 ka before gradually declining to a minimum of ~0.6 % at 120 ka (Figure 4).

253

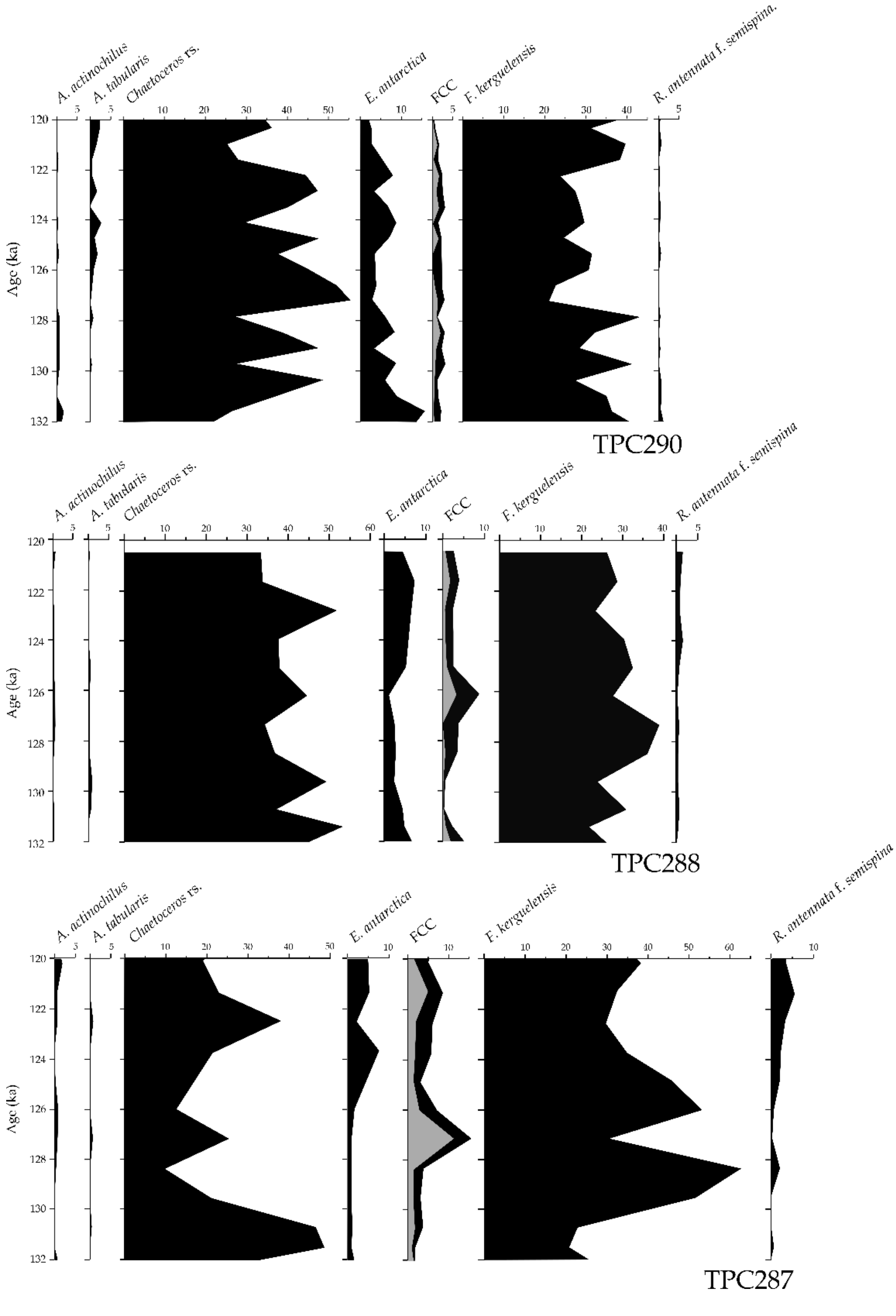

Figure 4: Downcore relative diatom abundances for the three Atlantic Sector cores (TPC290, TPC288 and TPC287) covering the 132-120 ka period. For the FCC group, the grey shading shows the *F. cylindrus* abundance and the black shading shows the *F. curta* abundance.

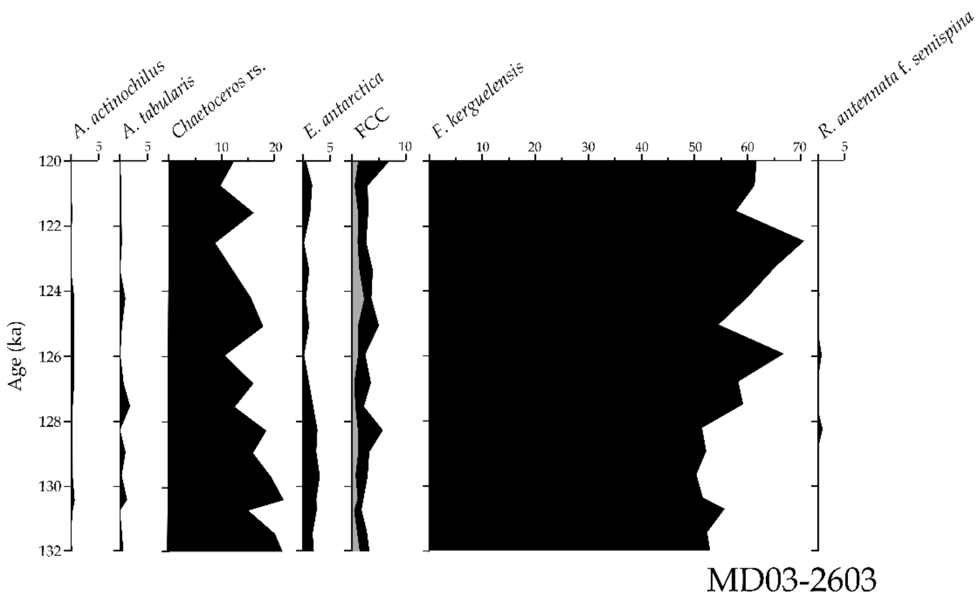

Figure 5: Downcore relative diatom abundances for the Indian Sector core (MD03-2603) covering the 132-120 ka period. For the FCC group, the grey shading shows the *F. cylindrus* abundance and the black shading shows the *F. curta* abundance.

In the Pacific Sector cores (ELT17-9, NBP9802-04 and PC509), the FCC abundances are largely uniform throughout MIS 5e, at ~2 %, ~3.5 % and ~6 % respectively (Figure 6). Cores ELT17-9 and NBP9802-04 reach a FCC abundance minimum of ~0.9 % at ~124 ka, whereas the minimum (4.5 %) in PC509 occurs earlier at ~129 ka, consistent with the more southerly Atlantic Sector cores (TPC288 and TPC287) (Figures 4 & 6). Core MD03-2603 also has a largely constant FCC abundance of ~3.5 % throughout MIS 5e, although it reaches minima of 1.7 % at ~130.5 ka and 2.2 % at ~127.5 ka, both of which are concurrent with *A. tabularis* abundance peaks of >1 % (Figure 5).

The *Eucampia antarctica* (cold variety) and *Rhizosolenia antennata* f. *semispina* abundances in TPC288 and TPC287 show coincident increases after 126 ka (Figure 4). This pattern is not seen in TPC290, where the *R. antennata* f. *semispina* abundance remains low (0.3 ± 0.4 %) throughout MIS 5e and the highest *E. antarctica* abundances (>10 %) are observed before 131 ka (Figure 4). In the four Indian and Pacific Sector cores both *R. antennata* f. *semispina* and *E. antarctica* have low abundances (<5 %) throughout the 132-120 ka interval (Figures 5 & 6).

5.2. <u>Comparison between Termination II-MIS 5e and recent diatom assemblages</u>

The diatom abundances in the surface sediments are compared with the average abundances in three Termination II-MIS 5e time slices – early (132-130 ka), mid (130-125 ka) and late (125-120 ka) (Table 6). These MIS 5e time windows are chosen to reconstruct average palaeoenvironmental conditions for the end of the deglaciation, the peak of MIS 5e and the later stage of MIS 5e, respectively, thereby

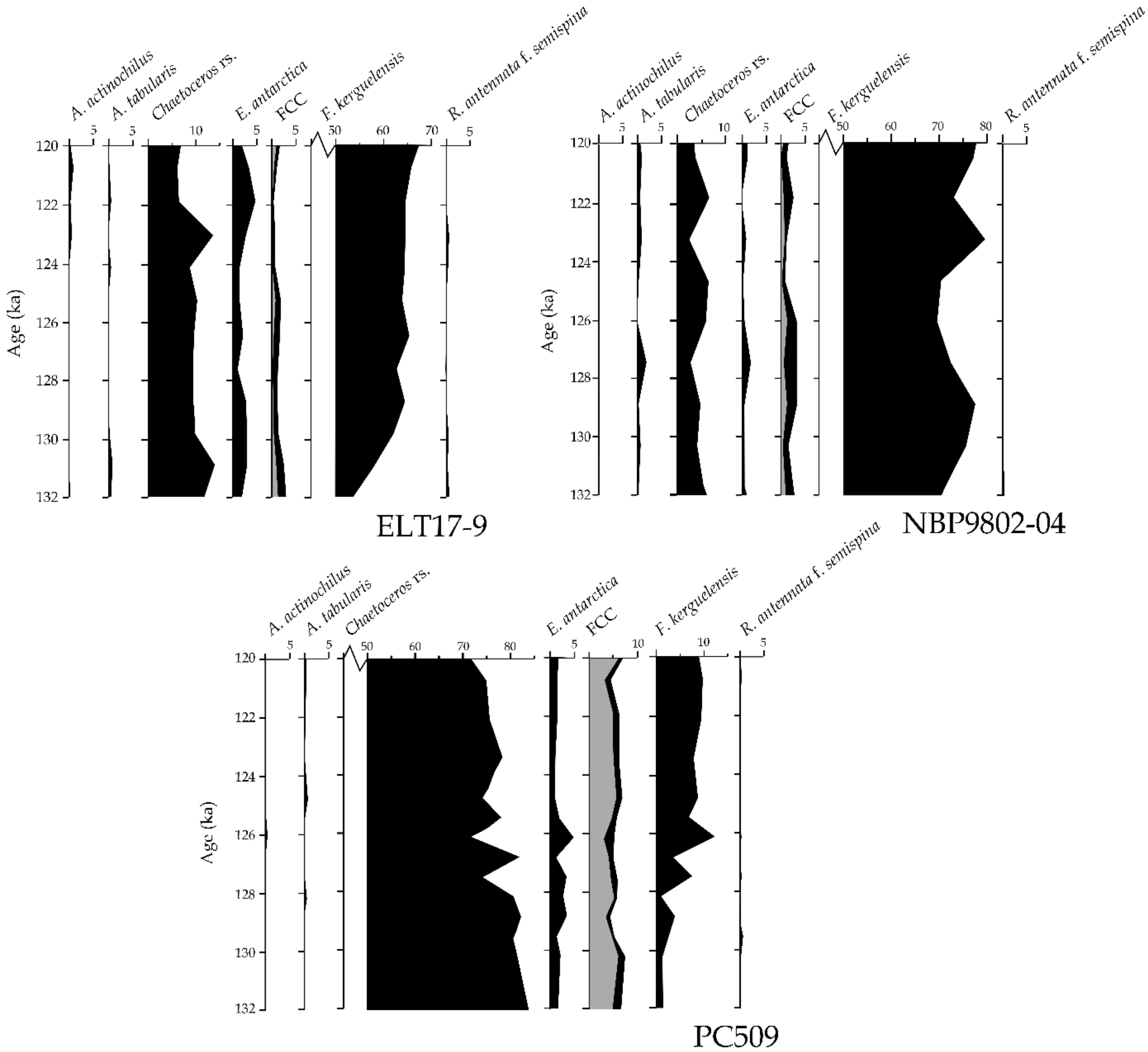

Figure 6: Downcore relative diatom abundances for the three Pacific Sector cores (ELT17-9, NBP9802-04 and PC509) covering the 132-120 ka period. For the FCC group, the grey shading shows the *F. cylindrus* abundance and the black shading shows the *F. curta* abundance. Note that the scales for species/groups with abundances >50 % of the assemblage throughout MIS 5e start at 50 %.

following the divisions suggested by Capron et al. (2014). To ensure there are data from at least 3 samples for each time slice, 1 sample older than 132 ka had to be included in the 132-130 ka window for five cores (TPC288, TPC287, ELT17-9, NBP9802-04 and PC509). Figures 7 & 8 show the differences in spatial and temporal relative abundances for four of the key groups (*Chaetoceros* rs., *E. antarctica*, FCC and *F. kerguelensis*) in the three Termination II-MIS 5e intervals and the surface sediments. Diatom assemblages in the surface sediments are consistent with the modern environmental setting.

A. actinochilus and *A. tabularis* have similar, but opposing, offsets (<1 %) between the surface sediments and the three time slices in all the cores (Table 6). The higher abundances of *A. tabularis* and lower abundances of *A. actinochilus* in the MIS 5e sediments when compared to the surface sediments supports the warmer than present conditions expected during MIS 5e (Capron et al. 2014). Care should be taken when interpreting such small changes in species abundance. However, because both *A. actinochilus* and *A. tabularis* occur in very low relative abundances (<3-5 %) throughout the Antarctic Zone of the SO (Armand et al. 2005, Romero et al. 2005, Esper et al. 2010), even small variations in their relative abundances, especially across multiple consecutive downcore sediment samples, can indicate substantial environmental shifts.

Most of the cores have largely similar *Chaetoceros* rs. abundances across all three time slices and in the surface sediments. Core TPC287 is a clear exception, with a decrease of >20 % between the early (42.5 %) and the mid and late time slices (17.2 % and 23.4 % respectively) (Figure 8). The modern *Chaetoceros* rs. abundance for TPC287 (33.3 %) is most similar to the early time slice (42.5 %) but is ~10 % different from any of the time slices (Figure 8). The combined abundance of *F. kerguelensis* and *Chaetoceros* rs. in TPC287 is very similar between the early and mid time slices (65.8 % and 66.7 % respectively) indicating that the decrease in *Chaetoceros* rs. is almost exactly matched by an increase in *F. kerguelensis* (Figure 4). This transition from a *Chaetoceros* rs. dominated assemblage during Termination II to a *F. kerguelensis* dominated one during the mid and late time slices is likely related to a change in the major oceanographic influence at this site. The stratified surface waters of the Weddell Gyre overly core site TPC287 (Vernet et al. 2019), and, thus, clockwise lateral transport of robust *Chaetoceros* rs. from the Antarctic Peninsula and Weddell Sea Embayment (Crosta et al. 1997) may have caused the high Chaetoceros rs. abundances in this core. A poleward shift of the northern boundary of the Weddell Gyre during MIS 5e, as indicated by multiple CMIP3 and CMIP5 models under a warmer than present climate (Meijers et al. 2012, Wang 2013), and the accompanying southerly displacement in surface water masses, would result in the replacement of high *Chaetoceros* rs. abundances with high *F. kerguelensis* abundances, indicative of open ocean conditions (Hasle 1969, Cefarelli et al. 2010). A reduction in the longitudinal extent of the Weddell Gyre during MIS 5e is supported by other core records from the SW Indian Sector (Ghadi et al. 2020). The Indian and Pacific Sector cores show similar *F. kerguelensis* abundance patterns with increasing abundances in the mid and late time slices (Figure 8). All cores for which a surface sample is available have greater *F. kerguelensis* abundances in the mid and late time slices than in the surface sediments (Figure 8), indicating increased open ocean conditions during MIS 5e.

Consistent with the evidence of increased open ocean conditions during MIS 5e, the FCC abundances in all cores indicate a reduced WSIE during MIS 5e relative to the surface sediments (Figure 8). All three Atlantic cores share similar patterns in FCC abundances, with the lowest abundances occurring during Termination II (average 2.1 %) followed by an increase during the mid time slice (average 4.5 %) and subsequent decrease during the late time slice (average 3.6 %) (Figure 8). The amplitude of these abundance changes exhibits a N-S trend with the highest amplitude shifts at the most southerly site (TPC287) and the least variation at the northernmost site (TPC290). The FCC abundances in core PC509 are consistently >3 % from 132 ka to 120 ka which indicates that the site was located to the south of the mean WSIE throughout this entire period (Figure 6). The two central Pacific Sector cores (ELT17-9 and NBP9802-04) do not have surface sediment assemblages to compare with. However, the FCC abundances (Figure 6) suggest that during Termination II and MIS 5e, site ELT17-9 (FCC ~1-2 %) was located on the edge of the maximum WSIE and site NBP9802-04 (FCC ~3 %) was located near the mean WSIE until 126 ka, when the winter sea-ice limit retreated. Compared to the modern September sea-ice extent (Figures 1, 7 & 8), the FCC abundances (Figure 8) indicate a southward shift in sea-ice cover for the central Pacific Sector during Termination II-MIS 5e. FCC abundances in core MD03-2603 show strong similarity between the mid and late time slices and the surface sediments (Figure 8). The greater WSIE reduction in the Atlantic Sector compared to the Pacific and Indian Sectors supports the pattern of the simulated MIS 5e WSIE minimum in Holloway et al. (2017).

The *E. antarctica* (cold variety) abundances are highest in cores TPC290 and TPC288 (5.5 % & 5.8 % respectively), whilst the Indian and Pacific Sector cores have low abundances throughout Termination II and MIS 5e (average 2.6 %) and the modern (average 1.5 %) (Figure 7). Higher *E. antarctica* abundances in the Atlantic Sector cores when compared to the Pacific and Indian Sector cores (Figure 5) are likely linked to greater influence of iceberg flux from the Weddell Sea Sector than the other Antarctic embayments (Death et al. 2014). The high *E. antarctica* abundances for the Termination II interval in cores TPC290 and TPC288 when compared to surface sediments (Table 6 & Figure 7) suggest a higher iceberg supply during the deglaciation, which is supported by high accumulation rates of iceberg-rafted debris during this time recorded in Weddell Sea cores from the East Antarctic margin (Diekmann et al. 2003). During the late time slice the high *E. antarctica* abundances (6.2 % and 5.1 %, respectively) in cores TPC288 and TPC287 indicate a later period of substantial iceberg flux, which could reflect a poleward migration and/or expansion of the iceberg tracks over the course of MIS 5e. A poleward displacement of the iceberg tracks would support a contraction of the Weddell Gyre (Tournadre et al. 2016) and suggest a southerly shift in the position of the ACC and wind fields (Gladstone et al. 2001). Present day iceberg trajectories support the greater *E. antarctica* abundance in the surface sediment assemblage of core TPC290 when compared with the *E. antarctica* abundance in surface sediments of cores TPC288 and TPC287 (Silva et al. 2006).

5.3. Environmental heterogeneity during MIS 5e

Peaks in *A. tabularis* abundance (~2 %) at ~127.5 ka in cores MD03-2603 and NBP9802-04 (Figures 5 & 6) and the increased *A. tabularis* abundance between 126-124 ka and 121-120 ka in core TPC290

(Figure 4) could be related to higher SSTs and a more southerly Polar Front than the modern. Poleward migration of the Polar Front in the Atlantic Sector during MIS 5e has been concluded from previously published proxy reconstructions (Nürnberg et al. 1997, Bianchi & Gersonde 2002, Howe et al. 2002, Kemp et al. 2010, Chadwick et al. 2020). Unlike NBP9802-04 and MD03-2603, the ELT17-9 and PC509 records have very low *A. tabularis* abundances throughout Termination II and MIS 5e (Figure 6) which suggests that, if there was a southerly migration in the Polar Front, it did not occur uniformly across the Pacific and Indian Sectors. Heterogeneous frontal migration during MIS 5e is supported by Chadwick et al. (2020), and is also evident for the modern SO (Freeman et al. 2016). It could be caused by the 'pinning' of fronts by bathymetric features in some regions, which will impede their migration (Nghiem et al. 2016).

The higher *R. antennata* f. *semispina* abundances in the most southerly Atlantic cores (TPC288 and TPC287, Figure 4) during the interval 126-120 ka indicate that the edge of the mean WSIE was closer to both core sites during this interval than during the rest of MIS 5e (cf. Crosta et al. 2005) and also indicate increased surface meltwater stratification (cf. Allen et al. 2005). This increased meltwater stratification could have resulted either from the annual melting at the mean WSIE (Armand & Leventer 2003) or melting associated with high iceberg flux indicated by the elevated *E. antarctica* abundances (Figures 4 & 7), with high global sea level after 126 ka (Kopp et al. 2013) supporting a large reduction in global ice volume at this time. The abundances of *E. antarctica,* FCC and *R. antennata* f. *semispina* during Termination II and MIS 5e document clear environmental differences between the largely stable conditions in the Pacific and Indian Sectors (Figures 5 & 6) and the more variable conditions in the southerly Atlantic Sector (cores TPC288 and TPC287, Figure 4). FCC abundances likely indicate an early (~130-129 ka) WSIE minimum at sites TPC288 and TPC287. This is consistent with the FCC records for cores MD03-2603 and PC509 (Figures 5 & 6) but the substantial re-expansion of WSIE at ~127-126 ka is only seen in the Atlantic Sector records (Figure 4). In the Indian Sector, the similarity in FCC abundances between the Termination II-MIS 5e and surface samples in core MD03-2603 (Figure 8) could be due to the influence of the Australian-Antarctic Basin gyre regulating the position of the WSIE along the Adélie Land margin in East Antarctica (McCartney & Donohue 2007, Carter et al. 2008).

	TPC290				TPC288				TPC287				ELT17-9			NBP9802-04			MD03-2603				PC509			
	132* – 130 ka	13 0– 125 ka	125 – 120 ka	Modern	132* – 130 ka	13 0– 125 ka	125 – 120 ka	Modern	132* – 130 ka	13 0– 125 ka	125 – 120 ka	Modern	132* – 130 ka	13 0– 125 ka	125 – 120 ka	132* – 130 ka	13 0– 125 ka	125 – 120 ka	132* – 130 ka	13 0– 125 ka	125 – 120 ka	Modern [a]	132* – 130 ka	13 0– 125 ka	125 – 120 ka	Modern
A. actinochilus	0.7	0.4	0.1	0.0	0.3	0.4	0.3	0.6	0.2	0.5	0.7	1.0	0.1	0.0	0.5	0.1	0.1	0.0	0.3	0.5	0.2	0.7	0.0	0.1	0.0	0.0
A. tabularis	0.0	0.5	1.2	0.0	0.2	0.5	0.1	0.0	0.1	0.2	0.1	0.3	0.6	0.0	0.4	0.4	0.8	0.7	0.6	0.6	0.4	0.7	0.0	0.1	0.3	0.0
***Chaetoceros* rs.**	38.6	42.5	38.1	46.8	45.2	40.9	39.4	39.0	42.5	17.2	23.4	33.3	12.0	9.7	8.8	6.2	4.6	4.9	19.1	16.1	12.6	12.5	82.9	78.6	76.0	73.5
E. antarctica	10.1	5.0	5.5	6.6	5.5	3.0	6.2	3.4	1.3	1.2	5.1	2.6	2.8	2.1	3.3	1.4	1.1	0.6	2.4	2.0	1.1	1.0	2.2	3.0	1.5	2.0
FCC	1.6	2.5	2.0	7.6	2.6	3.9	3.0	5.3	2.2	7.2	5.8	14.0	2.4	1.6	0.8	2.7	3.4	1.6	2.2	3.5	3.2	4.8	7.0	5.4	6.1	7.8
F. kerguelensis	33.4	31.9	30.7	20.8	23.8	30.2	24.7	23.9	23.3	49.5	37.0	16.6	57.9	64.1	64.9	71.8	73.5	75.3	55.1	58.4	66.3	56.1	1.5	5.5	9.1	5.1
R. antennata* f. *semispina	0.5	0.2	0.2	0.7	0.9	0.8	2.4	7.8	0.6	0.9	3.6	6.2	0.2	0.3	0.3	0.1	0.0	0.0	0.2	0.2	0.1	0.3	0.3	0.2	0.3	0.0

Table 6: Mean abundances for the three Termination II-MIS 5e time slices (early = 132*-130 ka; mid = 130-125 ka; late = 125-120 ka) at each core site and modern abundances in surface sediments. The 132*-130 ka time slice includes samples older than 132 ka in five of the cores (TPC288, TPC287, ELT17-9, NBP9802-04 and PC509).
[a] modern abundances for MD03-2603 are from the surface sediments at IODP Site U1361.

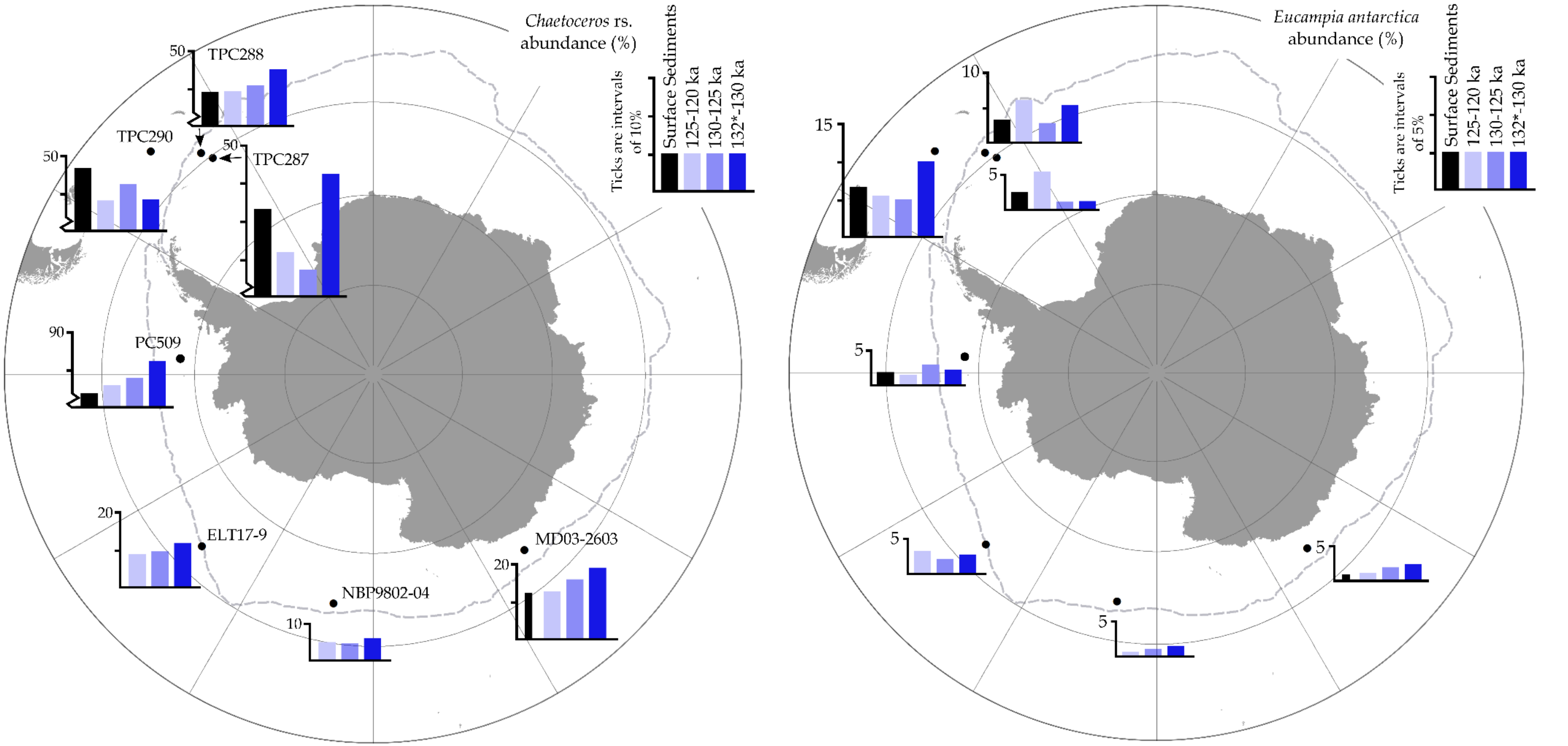

Figure 7: Maps of *Chaetoceros* rs. (LHS) and *Eucampia antarctica* (RHS) abundances in seven marine sediment cores. Modern diatom abundances are marked by black bars and mean abundances during three Termination II-MIS 5e time slices (early = 132*-130 ka; mid = 130-125 ka; late = 125-120 ka) are indicated by bars with different shades of blue. Thin black bars on the MD03-2603 graphs indicate diatom abundances in the surface sediment samples from the nearby IODP Site U1361. The black dots mark the core locations and the grey dashed line is the median modern (1981-2010) September sea-ice extent from Fetterer et al. (2017). *: the 132-130 ka time slice includes samples older than 132 ka to ensure that at least three samples are included in the average.

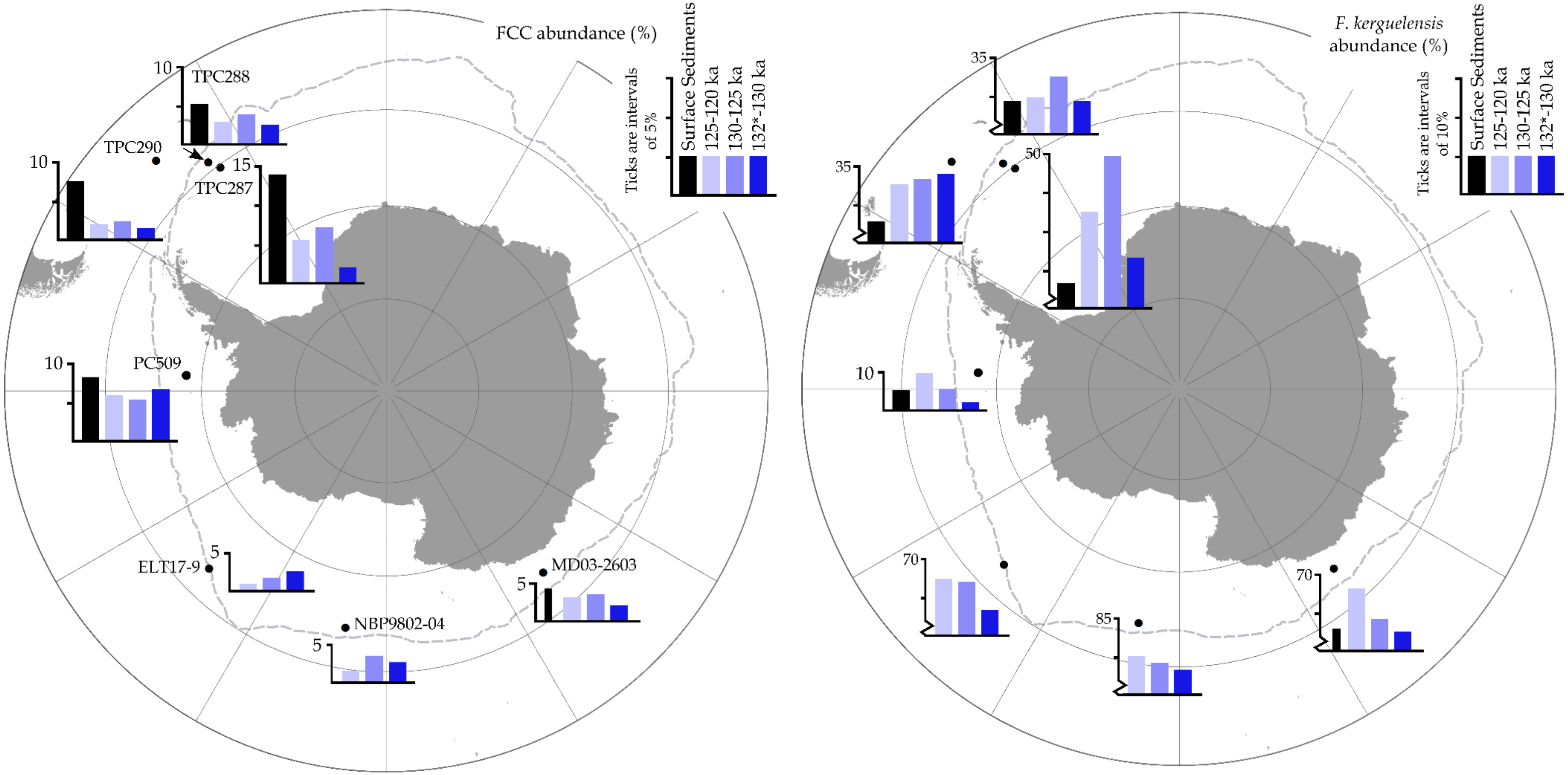

Figure 8: Maps of FCC (LHS) and *F. kerguelensis* (RHS) abundances in seven marine sediment cores. Modern diatom abundances are marked by black bars and mean abundances during three Termination II-MIS 5e time slices (early = 132*-130 ka; mid = 130-125 ka; late = 125-120 ka) are indicated by bars with different shades of blue. Thin black bars on the MD03-2603 graphs indicate diatom abundances in the surface sediment sample from the nearby IODP Site U1361. The black dots mark the core locations and the grey dashed line is the median modern (1981-2010) September sea-ice extent from Fetterer et al. (2017). *: the 132-130 ka time slice includes samples older than 132 ka to ensure that at least three samples are included in the average.

378

6. Conclusions and wider implications

The early (~130 ka) reduction in WSIE and increase in SSTs at the start of MIS 5e for the two most southerly Atlantic Sector cores (TPC288 and TPC287, Figure 4), coupled with the indication of a poleward contraction of the Weddell Gyre, have large implications for the region and further afield. The downwelling of dense water masses in the Weddell Sea is a key component in the formation of Antarctic Bottom Water (Orsi et al. 2002), which helps drive global ocean overturning circulation (Brix & Gerdes 2003). Reduced WSIE, with a winter sea-ice edge located further south than its modern position, resulted from less sea ice formation in coastal polynyas and from less sea ice advection to the north by winds and subsequent Ekman transport. This, in turn, suggests less brine rejection which may lead to a subsequent decrease in the rates of deep and bottom water mass production along the Antarctic coast as well as a warming of the abyssal waters (Bouttes et al. 2010, Ferrari et al. 2014, Marzocchi & Jansen 2019). Warmer surface and abyssal waters in the Weddell Sea would imply accelerated basal melting of ice shelves and increased grounding line retreat of marine terminating ice streams in the region, which in turn would induce substantial mass loss from the Antarctic ice sheets (Pollard & DeConto 2009, DeConto & Pollard 2016). This increased melting and ice sheet loss may account for the sea ice resurgence (Merino et al. 2018) and increased iceberg discharge (Liu et al. 2015) inferred from cores TPC288 and TPC287 after 127 ka (Figure 4). Surface water freshening from glacial meltwater input has also been linked to a reduction in the formation rates of Antarctic Bottom Water, causing further warming of the abyssal ocean (Fogwill et al. 2015, Lago & England 2019).

The possible southerly shifts in the Polar Front near sites NBP9802-04 and MD03-2603 and the poleward contraction of the Weddell Gyre south of site TPC287 suggest a poleward migration of the ACC during MIS 5e. A more southerly ACC causes increased advection of relatively warm ACC water masses, such as Circumpolar Deep Water, onto the Antarctic continental shelf (Fogwill et al. 2014, Spence et al. 2017). These warm upwelling ACC water masses contribute to the melting of glacial ice (Hellmer et al. 2012), similar to what is observed today in the Amundsen-Bellingshausen Sea sectors of West Antarctica (Rignot et al. 2019). A southern shift of the ACC would also have caused a poleward movement of the precipitation field and storm tracks (Liu & Curry 2010). A poleward migration of the precipitation field near site MD03-2603 would result in drier conditions across Southern Australia (Saunders et al. 2012), as seen today (CSIRO 2018).

Warming and reduced WSIE in the Weddell Sea could also have a substantial impact on the SO biosphere. At present, the Weddell Sea has the highest area-normalised primary productivity rates in the SO (Vernet et al. 2019). Reduced sea-ice extent and increased glacial meltwater supply during MIS 5e likely promoted greater primary productivity, as observed today (de Jong et al. 2012, Kahru et al.

2016). In contrast, Antarctic krill (*Euphausia superba*), a key trophic intermediary in the modern SO (Knox 2006), prefers lower water temperatures (Siegel & Watkins 2016, Atkinson et al. 2017). A repeat of warmer MIS 5e-like conditions in the future will therefore likely cause a substantial reduction in the habitat and abundances of Antarctic krill in the SO and impact the populations of megafauna that rely on them (Hill et al. 2013), as can be seen today in the rapidly warming northern region of the West Antarctic Peninsula (Montes-Hugo et al. 2009). A WSIE reduction in the Weddell Sea like during MIS 5e would also have damaging impacts for modern day sea-ice obligate species, e.g. Emperor Penguins (Jenouvrier et al. 2005).

The largely stable environmental conditions at the Pacific Sector core sites, especially ELT17-9, during Termination II-MIS 5e (Figure 6) suggest that this region may be more resilient to future changes. This is consistent with the observations that the modern WSIE in the central and western Pacific Sector is strongly influenced by the topography and bathymetry, through the pinning of fronts and currents (Nghiem et al. 2016). Greater stability of the WSIE in the Pacific Sector would have resulted in protection of ice shelves, such as the Ross Ice Shelf, and maintained their buttressing effect for grounded ice, similar to what is seen in present day Greenland (Walter et al. 2012). This could also have substantial implications for the stability of the West Antarctic Ice Sheet during MIS 5e, with no evidence in the PC509 record (Figure 6) of high iceberg flux originating from glaciers draining the Bellingshausen Sea Sector of the West Antarctic Ice Sheet (Gardner et al. 2018).

It is clear that, similar to today (Hobbs et al. 2016, Parkinson 2019), changes to the SO during MIS 5e were not spatially and temporally homogeneous. Some of the climatic variability during Termination II and MIS 5e is due to the difference in the topographic characteristics and oceanographic conditions, with the stability in the Pacific and East Indian Sectors likely due to bathymetry pinning and the stability of the Australian-Antarctic Basin gyre, respectively. This variation in the controls on and magnitude of changes in the Antarctic and SO climate system are important factors to be included into model simulations of future warming. MIS 5e is a valuable 'laboratory' for understanding how the Antarctic and SO region responds to a warmer climate, especially for regions like the Weddell Sea, where climatic trends during MIS 5e diverge from what is observed today (Purich et al. 2016, Parkinson 2019).

Data availability

Termination II and MIS 5e diatom assemblage data for all samples are available from the Polar Data Centre (Chadwick & Allen 2021a, b, c, d, e, f, g) and surface sediment diatom assemblages can be found at http://dx.doi.org/10.17632/2tnxcww6c8.1 an open-source online data repository hosted at Mendeley Data (Chadwick 2020).

Acknowledgements

We thank the captains, officers and crews as well as the science parties of the expeditions that collected the analysed cores. The British Ocean Sediment Core Research Facility (BOSCORF) is thanked for supplying sediment samples for core TPC287 and multi-sensor core logging of core PC509. We thank the Lamont-Doherty Core Repository of Lamont-Doherty Earth Observatory for providing sediment sample material for core NBP9802-04 (IGSN – DSR0003YW). The International Ocean Discovery Program (IODP) is thanked for providing the sample material from Hole U1361A. We also thank the Oregon State University Marine and Geology Repository for providing sediment samples for core ELT17-9. Mark Evans and Victoria Alcock are thanked for their assistance in the splitting and sampling of core PC509. We also thank two anonymous reviewers and the journal editor for their supportive and constructive reviews.

Funding

This work was supported by the Natural Environmental Research Council [grant number NE/L002531/1] and contributes to British Antarctic Survey's 'Polar Science for Planet Earth' program.

References

Abernathey R.P., Cerovecki I., Holland P.R., Newsom E., Mazloff M. & Talley L.D. 2016. Water-mass transformation by sea ice in the upper branch of the Southern Ocean overturning. *Nature Geoscience*, **9** (8): 596-601.

Allen C.S. 2014. Proxy development: a new facet of morphological diversity in the marine diatom *Eucampia antarctica* (Castracane) Mangin. *Journal of Micropalaeontology*, **33** (2): 131-142.

Allen C.S., Pike J., Pudsey C.J. & Leventer A. 2005. Submillennial variations in ocean conditions during deglaciation based on diatom assemblages from the southwest Atlantic. *Paleoceanography*, **20** (2): 1-16.

Armand L. & Leventer A. 2003. Palaeo Sea Ice Distribution - Reconstruction and Palaeoclimatic Significance. In: *Sea Ice: An Introduction to its Physics, Chemistry, Biology and Geology***:** 333-372.

Armand L.K., Crosta X., Romero O. & Pichon J.-J. 2005. The biogeography of major diatom taxa in Southern Ocean sediments: 1. Sea ice related species. *Palaeogeography, Palaeoclimatology, Palaeoecology*, **223** (1-2): 93-126.

Armand L.K. & Zielinski U. 2001. Diatom species of the genus *Rhizosolenia* from Southern Ocean sediments: distribution and taxonomic notes. *Diatom Research*, **16** (2): 259-294.

Atkinson A., Hill S.L., Pakhomov E.A., Siegel V., Anadon R., Chiba S., Daly K.L., Downie R., Fielding S., Fretwell P., Gerrish L., Hosie G.W., Jessopp M.J., Kawaguchi S., Krafft B.A., Loeb V., Nishikawa J., Peat H.J., Reiss C.S., Ross R.M., Quetin L.B., Schmidt K., Steinberg D.K., Subramaniam R.C., Tarling G.A. & Ward P. 2017. KRILLBASE: a circumpolar database of Antarctic krill and salp numerical densities, 1926–2016. *Earth System Science Data*, **9** (1): 193-210.

Barbara L., Crosta X., Leventer A., Schmidt S., Etourneau J., Domack E. & Massé G. 2016. Environmental responses of the Northeast Antarctic Peninsula to the Holocene climate variability. *Paleoceanography*, **31** (1): 131-147.

Beans C., Hecq J.H., Koubbi P., Vallet C., Wright S. & Goffart A. 2008. A study of the diatom-dominated microplankton summer assemblages in coastal waters from Terre Adélie to the Mertz Glacier, East Antarctica (139°E–145°E). *Polar Biology*, **31** (9): 1101-1117.

Bianchi C. & Gersonde R. 2002. The Southern Ocean surface between Marine Isotope Stages 6 and 5d: Shape and timing of climate changes. *Palaeogeography, Palaeoclimatology, Palaeoecology*, **187**: 151-177.

Bouttes N., Paillard D. & Roche D.M. 2010. Impact of brine-induced stratification on the glacial carbon cycle. *Climate of the Past*, **6** (5): 575-589.

Brathauer U., Abelmann A., Gersonde R., Niebler H.S. & Fütterer D.K. 2001. Calibration of *Cycladophora davisiana* events versus oxygen isotope stratigraphy in the subantarctic Atlantic Ocean - a stratigraphic tool for carbonate-poor Quaternary sediments. *Marine Geology*, **175**: 167-181.

Brix H. & Gerdes R. 2003. North Atlantic Deep Water and Antarctic Bottom Water: Their interaction and influence on the variability of the global ocean circulation. *Journal of Geophysical Research: Oceans*, **108** (C2): 3022.

Burckle L.H. 1984. Ecology and paleoecology of the marine diatom *Eucampia antarctica* (Castr.) Mangin. *Marine Micropaleontology*, **9**: 77-86.

Burckle L.H. & Burak R.W. 1995. Relative abundance of *Eucampia antarctica* as a close proxy to $\delta^{18}O$ in upper Quaternary sediments of the Southern Ocean. In: *Landscapes and Life: Studies in Honour of Urve Miller*, Robertsson A.M. Ed. Cons. de L'Eur., Rixensart, Belgium**:** 15-22.

Burckle L.H., Clarke D.B. & Shackleton N.J. 1978. Isochronous last-abundant-appearance datum (LAAD) of the diatom *Hemidiscus karstenii* in the sub-Antarctic. *Geology*, **6**: 243-246.

Busch W.H. 1991. Analysis of wet-bulk density and sediment color cycles in Pliocene-Pleistocene sediments of the Owen Ridge (Site 722) and Oman Margin (Site 728). In: *Proceedings of the Ocean Drilling Program, Scientific Results*, Prell W.J. & Niitsuma N. Eds., College Station, TX (Ocean Drilling Program). **117:** 239-253.

Capron E., Govin A., Feng R., Otto-Bliesner B.L. & Wolff E.W. 2017. Critical evaluation of climate syntheses to benchmark CMIP6/PMIP4 127 ka Last Interglacial simulations in the high-latitude regions. *Quaternary Science Reviews*, **168**: 137-150.

Capron E., Govin A., Stone E.J., Masson-Delmotte V., Mulitza S., Otto-Bliesner B., Rasmussen T.L., Sime L.C., Waelbroeck C. & Wolff E.W. 2014. Temporal and spatial structure of multi-millennial temperature changes at high latitudes during the Last Interglacial. *Quaternary Science Reviews*, **103**: 116-133.

Carter L., McCave I.N. & Williams M.J.M. 2008. Circulation and Water Masses of the Southern Ocean: A Review. In: *Developments in Earth & Environmental Sciences*, Florindo F. & Siegert M. Eds. Elsevier, Amsterdam. **8:** 85-114.

Cefarelli A.O., Ferrario M.E., Almandoz G.O., Atencio A.G., Akselman R. & Vernet M. 2010. Diversity of the diatom genus *Fragilariopsis* in the Argentine Sea and Antarctic waters: morphology, distribution and abundance. *Polar Biology*, **33** (11): 1463-1484.

Chadwick M. 2020. Southern Ocean surface sediment diatom abundances. *Mendeley Data*.

Chadwick M. & Allen C.S. 2021a. Marine Isotope Stage 5e diatom assemblages in marine sediment core ELT17-9 (-63.08 °N, -135.12 °E, Cruise ELT17). *UK Polar Data Centre, Natural Environment Research Council, UK Research & Innovation*.

Chadwick M. & Allen C.S. 2021b. Marine Isotope Stage 5e diatom assemblages in marine sediment core MD03-2603 (-64.28 °N, 139.38 °E, Cruise MD130) *UK Polar Data Centre, Natural Environment Research Council, UK Research & Innovation*.

Chadwick M. & Allen C.S. 2021c. Marine Isotope Stage 5e diatom assemblages in marine sediment core NBP9802-04 (-64.20 °N, -170.08 °E, Cruise PA9802) *UK Polar Data Centre, Natural Environment Research Council, UK Research & Innovation*.

Chadwick M. & Allen C.S. 2021d. Marine Isotope Stage 5e diatom assemblages in marine sediment core PC509 (-68.31 °N, -86.03 °E, Cruise JR179). *UK Polar Data Centre, Natural Environment Research Council, UK Research & Innovation*.

Chadwick M. & Allen C.S. 2021e. Marine Isotope Stage 5e diatom assemblages in marine sediment core TPC287 (-60.31 °N, -36.65 °E, Cruise JR48) *UK Polar Data Centre, Natural Environment Research Council, UK Research & Innovation*.

Chadwick M. & Allen C.S. 2021f. Marine Isotope Stage 5e diatom assemblages in marine sediment core TPC288 (-59.14 °N, -37.96 °E, Cruise JR48) *UK Polar Data Centre, Natural Environment Research Council, UK Research & Innovation*.

Chadwick M. & Allen C.S. 2021g. Marine Isotope Stage 5e diatom assemblages in marine sediment core TPC290 (-55.55 °N, -45.02 °E, Cruise JR48). *UK Polar Data Centre, Natural Environment Research Council, UK Research & Innovation*.

Chadwick M., Allen C.S., Sime L.C. & Hillenbrand C.D. 2020. Analysing the timing of peak warming and minimum winter sea-ice extent in the Southern Ocean during MIS 5e. *Quaternary Science Reviews*, **229**: 106134.

Chase Z., Anderson R.F., Fleisher M.Q. & Kubik P.W. 2003. Accumulation of biogenic and lithogenic material in the Pacific sector of the Southern Ocean during the past 40,000 years. *Deep-Sea Research Part II: Topical Studies in Oceanography*, **50** (3-4): 799-832.

Cortese G., Dunbar G.B., Carter L., Scott G., Bostock H., Bowen M., Crundwell M., Hayward B.W., Howard W., Martínez J.I., Moy A., Neil H., Sabaa A. & Sturm A. 2013. Southwest Pacific Ocean response to a warmer world: Insights from Marine Isotope Stage 5e. *Paleoceanography*, **28** (3): 585-598.

Crosta X., Pichon J.-J. & Labracherie M. 1997. Distribution of *Chaetoceros* resting spores in modern peri-Antarctic sediments. *Marine Micropaleontology*, **29**: 283-299.

Crosta X., Pichon J.J. & Burckle L.H. 1998. Application of modern analog technique to marine Antarctic diatoms: Reconstruction of maximum sea-ice extent at the Last Glacial Maximum. *Paleoceanography*, **13** (3): 284-297.

Crosta X., Romero O., Armand L.K. & Pichon J.-J. 2005. The biogeography of major diatom taxa in Southern Ocean sediments: 2. Open ocean related species. *Palaeogeography, Palaeoclimatology, Palaeoecology*, **223** (1-2): 66-92.

CSIRO. 2018. State of the Climate. Australia, Bureau of Meteorology, 1-24.

de Jong J., Schoemann V., Lannuzel D., Croot P., de Baar H. & Tison J.-L. 2012. Natural iron fertilization of the Atlantic sector of the Southern Ocean by continental shelf sources of the Antarctic Peninsula. *Journal of Geophysical Research: Biogeosciences*, **117**: G01029.

Death R., Wadham J.L., Monteiro F., Le Brocq A.M., Tranter M., Ridgwell A., Dutkiewicz S. & Raiswell R. 2014. Antarctic ice sheet fertilises the Southern Ocean. *Biogeosciences*, **11** (10): 2635-2643.

DeConto R.M. & Pollard D. 2016. Contribution of Antarctica to past and future sea-level rise. *Nature*, **531** (7596): 591-597.

Diekmann B., Futterer D., Grobe H., Hillenbrand C.-D., Kuhn G., Michels K., Petschick R. & Pirrung M. 2003. Terrigenous Sediment Supply in the Polar to Temperate South Atlantic: Land-Ocean Links of Environmental Changes during the Late Quaternary. In: *The South Atlantic in the Late Quaternary: Reconstruction of Material Budgets and Current Systems*, Wefer G., Mulitza S. & Ratmeyer V. Eds. Springer-Verlag Berlin**:** 375-399.

Dong S., Sprintall J. & Gille S.T. 2006. Location of the Antarctic Polar Front from AMSR-E Satellite Sea Surface Temperature Measurements. *Journal of Physical Oceanography*, **36**: 2075-2089.

Esper O. & Gersonde R. 2014a. New tools for the reconstruction of Pleistocene Antarctic sea ice. *Palaeogeography, Palaeoclimatology, Palaeoecology*, **399**: 260-283.

Esper O. & Gersonde R. 2014b. Quaternary surface water temperature estimations: New diatom transfer functions for the Southern Ocean. *Palaeogeography, Palaeoclimatology, Palaeoecology*, **414**: 1-19.

Esper O., Gersonde R. & Kadagies N. 2010. Diatom distribution in southeastern Pacific surface sediments and their relationship to modern environmental variables. *Palaeogeography, Palaeoclimatology, Palaeoecology*, **287** (1-4): 1-27.

Ferrari R., Jansen M.F., Adkins J.F., Burke A., Stewart A.L. & Thompson A.F. 2014. Antarctic sea ice control on ocean circulation in present and glacial climates. *Proc Natl Acad Sci U S A*, **111** (24): 8753-8758.

Fetterer F., Knowles K., Meier W.N., Savoie M. & Windnagel A.K. 2017. Sea Ice Index, Version 3. *Boulder, Colorado USA*. NSIDC: National Snow and Ice Data Center.

Fischer H., Meissner K.J., Mix A.C., Abram N.J., Austermann J., Brovkin V., Capron E., Colombaroli D., Daniau A.-L., Dyez K.A., Felis T., Finkelstein S.A., Jaccard S.L., McClymont E.L., Rovere A., Sutter J., Wolff E.W., Affolter S., Bakker P., Ballesteros-Cánovas J.A., Barbante C., Caley T., Carlson A.E., Churakova O., Cortese G., Cumming B.F., Davis B.A.S., de Vernal A., Emile-Geay J., Fritz S.C. et al. 2018. Palaeoclimate constraints on the impact of 2 °C anthropogenic warming and beyond. *Nature Geoscience*, **11** (7): 474-485.

Fogwill C.J., Phipps S.J., Turney C.S.M. & Golledge N.R. 2015. Sensitivity of the Southern Ocean to enhanced regional Antarctic ice sheet meltwater input. *Earth's Future*, **3** (10): 317-329.

Fogwill C.J., Turney C.S.M., Meissner K.J., Golledge N.R., Spence P., Roberts J.L., England M.H., Jones R.T. & Carter L. 2014. Testing the sensitivity of the East Antarctic Ice Sheet to Southern Ocean dynamics: past changes and future implications. *Journal of Quaternary Science*, **29** (1): 91-98.

Freeman N.M., Lovenduski N.S. & Gent P.R. 2016. Temporal variability in the Antarctic Polar Front (2002-2014). *Journal of Geophysical Research: Oceans*, **121**: 7263-7276.

Fryxell G.A. & Prasad A.K.S.K. 1990. *Eucampia antarctica* var. *recta* (Mangin) stat. nov. (Biddulphiaceae, Bacillariophyceae): life stages at the Weddell Sea ice edge. *Phycologia*, **29** (1): 27-38.

Gardner A.S., Moholdt G., Scambos T., Fahnstock M., Ligtenberg S., van den Broeke M. & Nilsson J. 2018. Increased West Antarctic and unchanged East Antarctic ice discharge over the last 7 years. *The Cryosphere*, **12** (2): 521-547.

Gersonde R., Crosta X., Abelmann A. & Armand L. 2005. Sea-surface temperature and sea ice distribution of the Southern Ocean at the EPILOG Last Glacial Maximum—a circum-Antarctic view based on siliceous microfossil records. *Quaternary Science Reviews*, **24** (7-9): 869-896.

Gersonde R. & Zielinski U. 2000. The reconstruction of late Quaternary Antarctic sea-ice distribution—the use of diatoms as a proxy for sea-ice. *Palaeogeography, Palaeoclimatology, Palaeoecology*, **162**: 263-286.

Ghadi P., Nair A., Crosta X., Mohan R., Manoj M.C. & Meloth T. 2020. Antarctic sea-ice and palaeoproductivity variation over the last 156,000 years in the Indian sector of Southern Ocean. *Marine Micropaleontology*, **160**: 101894.

Gladstone R.M., Bigg G.R. & Nicholls K.W. 2001. Iceberg trajectory modeling and meltwater injection in the Southern Ocean. *Journal of Geophysical Research: Oceans*, **106** (C9): 19903-19915.

Govin A., Capron E., Tzedakis P.C., Verheyden S., Ghaleb B., Hillaire-Marcel C., St-Onge G., Stoner J.S., Bassinot F., Bazin L., Blunier T., Combourieu-Nebout N., El Ouahabi A., Genty D., Gersonde R., Jimenez-Amat P., Landais A., Martrat B., Masson-Delmotte V., Parrenin F., Seidenkrantz M.S., Veres D., Waelbroeck C. & Zahn R. 2015. Sequence of events from the onset to the demise of the Last Interglacial: Evaluating strengths and limitations of chronologies used in climatic archives. *Quaternary Science Reviews*, **129**: 1-36.

Govin A., Michel E., Labeyrie L., Waelbroeck C., Dewilde F. & Jansen E. 2009. Evidence for northward expansion of Antarctic Bottom Water mass in the Southern Ocean during the last glacial inception. *Paleoceanography*, **24** (1): PA1202.

Hasle G.R. 1969. *An analysis of the phytoplankton of the Pacific Southern Ocean: abundance, composition, and distribution during the Brategg Expedition, 1947-1948.*

Hellmer H.H., Kauker F., Timmermann R., Determann J. & Rae J. 2012. Twenty-first-century warming of a large Antarctic ice-shelf cavity by a redirected coastal current. *Nature*, **485** (7397): 225-228.

Hill S.L., Phillips T. & Atkinson A. 2013. Potential Climate Change Effects on the Habitat of Antarctic Krill in the Weddell Quadrant of the Southern Ocean. *PLoS One*, **8** (8): e72246.

Hillenbrand C.D., Kuhn G. & Frederichs T. 2009. Record of a Mid-Pleistocene depositional anomaly in West Antarctic continental margin sediments: an indicator for ice-sheet collapse? *Quaternary Science Reviews*, **28** (13-14): 1147-1159.

Hobbs W.R., Massom R., Stammerjohn S., Reid P., Williams G. & Meier W. 2016. A review of recent changes in Southern Ocean sea ice, their drivers and forcings. *Global and Planetary Change*, **143**: 228-250.

Hoffman J.S., Clark P.U., Parnell A.C. & Feng H. 2017. Regional and global sea-surface temperatures during the last interglaciation. *Science*, **355**: 276-279.

Holloway M.D., Sime L.C., Allen C.S., Hillenbrand C.-D., Bunch P., Wolff E. & Valdes P.J. 2017. The spatial structure of the 128 ka Antarctic sea ice minimum. *Geophysical Research Letters*, **44** (21): 11129-11139.

Howe J.A., Harland R. & Pudsey C.J. 2002. Dinoflagellate cyst evidence for Quaternary palaeoceanographic change in the northern Scotia Sea, South Atlantic Ocean. *Marine Geology*, **191**: 55-69.

IPCC. 2019. Summary for Policymakers. In: *IPCC Special Report on the Ocean and Cryosphere in a Changing Climate*, Portner H.O., Roberts D.C., Masson-Delmotte V. et al. Eds.**:** 1-36.

Jenouvrier S., Barbraud C. & Weimerskirch H. 2005. Long-term contrasted responses to climate of two Antarctic seabird species. *Ecology*, **86** (11): 2889-2903.

Kahru M., Lee Z., Mitchell B.G. & Nevison C.D. 2016. Effects of sea ice cover on satellite-detected primary production in the Arctic Ocean. *Biol Lett*, **12** (11): 20160223.

Kang S.-H. & Fryxell G.A. 1992. *Fragilariopsis cylindrus* (Grunow) Krieger: The most abundant diatom in water column assemblages of Antarctic marginal ice-edge zones *Polar Biology*, **12** (6-7): 609-627.

Kemp A.E.S., Grigorov I., Pearce R.B. & Naveira Garabato A.C. 2010. Migration of the Antarctic Polar Front through the mid-Pleistocene transition: evidence and climatic implications. *Quaternary Science Reviews*, **29** (17-18): 1993-2009.

King J. 2014. A resolution of the Antarctic paradox. *Nature*, **505**: 491-492.

Knox G.A. 2006. *Biology of the Southern Ocean*. Marine Biology Series: CRC Press.

Kopp R.E., Simons F.J., Mitrovica J.X., Maloof A.C. & Oppenheimer M. 2009. Probabilistic assessment of sea level during the last interglacial stage. *Nature*, **462** (7275): 863-867.

Kopp R.E., Simons F.J., Mitrovica J.X., Maloof A.C. & Oppenheimer M. 2013. A probabilistic assessment of sea level variations within the last interglacial stage. *Geophysical Journal International*, **193** (2): 711-716.

Lago V. & England M.H. 2019. Projected Slowdown of Antarctic Bottom Water Formation in Response to Amplified Meltwater Contributions. *Journal of Climate*, **32** (19): 6319-6335.

Leventer A. 1991. Sediment trap diatom assemblages from the northern Antarctic Peninsula region. *Deep-Sea Research*, **38** (89): 1127-1143.

Leventer A. 1992. Modern distribution of diatoms in sediments from the George V Coast, Antarctica. *Marine Micropaleontology*, **19**: 315-332.

Leventer A. & Dunbar R.B. 1988. Recent Diatom Record of McMurdo Sound, Antarctica: Implications for History of Sea Ice Extent. *Paleoceanography*, **3** (3): 259-274.

Lisiecki L.E. & Raymo M.E. 2005. A Pliocene-Pleistocene stack of 57 globally distributed benthic δ18O records. *Paleoceanography*, **20** (1): PA1003.

Liu J. & Curry J.A. 2010. Accelerated warming of the Southern Ocean and its impacts on the hydrological cycle and sea ice. *Proc Natl Acad Sci USA*, **107** (34): 14987-14992.

Liu Y., Moore J.C., Cheng X., Gladstone R.M., Bassis J.N., Liu H., Wen J. & Hui F. 2015. Ocean-driven thinning enhances iceberg calving and retreat of Antarctic ice shelves. *Proc Natl Acad Sci USA*, **112** (11): 3263-3268.

Maheshwari M., Singh R.K., Oza S.R. & Kumar R. 2013. An Investigation of the Southern Ocean Surface Temperature Variability Using Long-Term Optimum Interpolation SST Data. *ISRN Oceanography*, **2013**: 1-9.

Marzocchi A. & Jansen M.F. 2019. Global cooling linked to increased glacial carbon storage via changes in Antarctic sea ice. *Nature Geoscience*, **12**: 1001-1005.

McCartney M.S. & Donohue K.A. 2007. A deep cyclonic gyre in the Australian - Antarctic Basin. *Progress in Oceanography*, **75**: 675-750.

Meijers A.J.S., Shuckburgh E., Bruneau N., Sallee J.B., Bracegirdle T.J. & Wang Z. 2012. Representation of the Antarctic Circumpolar Current in the CMIP5 climate models and future changes under warming scenarios. *Journal of Geophysical Research: Oceans*, **117**: C12008.

Meinen C.S., Luther D.S., Watts D.R., Chave A.D. & Tracey K.L. 2003. Mean stream coordinates structure of the Subantarctic Front: Temperature, salinity, and absolute velocity. *Journal of Geophysical Research*, **108** (C8): 3263.

Merino N., Jourdain N.C., Le Sommer J., Goosse H., Mathiot P. & Durand G. 2018. Impact of increasing antarctic glacial freshwater release on regional sea-ice cover in the Southern Ocean. *Ocean Modelling*, **121**: 76-89.

Miklasz K.A. & Denny M.W. 2010. Diatom sinkings speeds: Improved predictions and insight from a modified Stokes' law. *Limnology and Oceanography*, **55** (6): 2513-2525.

Montes-Hugo M., Doney S.C., Ducklow H.W., Fraser W., Martinson D., Stammerjohn S.E. & Schofield O. 2009. Recent changes in phytoplankton communities associated with rapid regional climate change along the western Antarctic Peninsula. *Science*, **323** (5920): 1470-1473.

Nghiem S.V., Rigor I.G., Clemente-Colón P., Neumann G. & Li P.P. 2016. Geophysical constraints on the Antarctic sea ice cover. *Remote Sensing of Environment*, **181**: 281-292.

Nürnberg C.C., Bohrmann G., Schlüter M. & Frank M. 1997. Barium accumulation in the Atlantic sector of the Southern Ocean: Results From 190,000-year records. *Paleoceanography*, **12** (4): 594-603.

Orsi A.H., Smethie Jr. W.M. & Bullister J.L. 2002. On the total input of Antarctic waters to the deep ocean: A preliminary estimate from chlorofluorocarbon measurements. *Journal of Geophysical Research*, **107** (C8): 3122.

Orsi A.H., Whitworth III T. & Nowlin Jr W.D. 1995. On the meridional extent and fronts of the Antarctic Circumpolar Current. *Deep-Sea Research I*, **42** (5): 641-673.

Otto-Bliesner B.L., Rosenbloom N., Stone E.J., McKay N.P., Lunt D.J., Brady E.C. & Overpeck J.T. 2013. How warm was the last interglacial? New model-data comparisons. *Philos Trans A Math Phys Eng Sci*, **371** (2001): 20130097.

Paillard D., Labeyrie L. & Yiou P. 1996. Macintosh program performs time-series analysis. *Eos*, **77**: 379.

Parkinson C.L. 2019. A 40-y record reveals gradual Antarctic sea ice increases followed by decreases at rates far exceeding the rates seen in the Arctic. *Proc Natl Acad Sci USA*, **116** (29): 14414-14423.

Parrenin F., Barnola J.-M., Beer J., Blunier T., Castellano E., Chappellaz J., Dreyfus G., Fischer H., Fujita S., Jouzel J., Kawamura K., Lemieux-Dudon B., Loulergue L., Masson-Delmotte V., Narcisi B., Petit J.-R., Raisbeck G., Raynaud D., Ruth U., Schwander J., Severi M., Spahni R., Steffensen J.P., Svensson A., Udisti R., Waelbroeck C. & Wolff E. 2007. The EDC3 chronology for the EPICA Dome C ice core. *Climate of the Past*, **3**: 485-497.

Parrenin F., Masson-Delmotte V., Kohler P., Raynaud D., Paillard D., Schwander J., Barbante C., Landais A., Wegner A. & Jouzel J. 2013. Synchronisation of the LR04 stack with EDC isotopic variations on the EDC3 age scale. *PANGAEA*.

Pollard D. & DeConto R.M. 2009. Modelling West Antarctic ice sheet growth and collapse through the past five million years. *Nature*, **458** (7236): 329-332.

Presti M., Barbara L., Denis D., Schmidt S., De Santis L. & Crosta X. 2011. Sediment delivery and depositional patterns off Adélie Land (East Antarctica) in relation to late Quaternary climatic cycles. *Marine Geology*, **284** (1-4): 96-113.

Pugh R.S., McCave I.N., Hillenbrand C.D. & Kuhn G. 2009. Circum-Antarctic age modelling of Quaternary marine cores under the Antarctic Circumpolar Current: Ice-core dust–magnetic correlation. *Earth and Planetary Science Letters*, **284** (1-2): 113-123.

Purich A., England M.H., Cai W., Chikamoto Y., Timmermann A., Fyfe J.C., Frankcombe L., Meehl G.A. & Arblaster J.M. 2016. Tropical Pacific SST Drivers of Recent Antarctic Sea Ice Trends. *Journal of Climate*, **29** (24): 8931-8948.

Rignot E., Mouginot J., Scheuchl B., van den Broeke M., van Wessem M.J. & Morlighem M. 2019. Four decades of Antarctic Ice Sheet mass balance from 1979-2017. *Proc Natl Acad Sci USA*, **116** (4): 1095-1103.

Romero O.E., Armand L.K., Crosta X. & Pichon J.J. 2005. The biogeography of major diatom taxa in Southern Ocean surface sediments: 3. Tropical/Subtropical species. *Palaeogeography, Palaeoclimatology, Palaeoecology*, **223** (1-2): 49-65.

Rosenblum E. & Eisenman I. 2017. Sea Ice Trends in Climate Models Only Accurate in Runs with Biased Global Warming. *Journal of Climate*, **30** (16): 6265-6278.

Saunders K.M., Kamenik C., Hodgson D.A., Hunziker S., Siffert L., Fischer D., Fujak M., Gibson J.A.E. & Grosjean M. 2012. Late Holocene changes in precipitation in northwest Tasmania and their potential links to shifts in the Southern Hemisphere westerly winds. *Global and Planetary Change*, **92-93**: 82-91.

Scherer R.P. 1994. A new method for the determination of absolute abundance of diatoms and other silt-sized sedimentary particles. *Journal of Paleolimnology*, **12** (2): 171-179.

Schmidtko S., Heywood K.J., Thompson A.F. & Aoki S. 2014. Multidecadal warming of Antarctic waters. *Science*, **346** (6214): 1227-1231.

Siegel V. & Watkins J.L. 2016. Distribution, Biomass and Demography of Antarctic Krill, *Euphausia superba*. In: *Biology and Ecology of Antarctic krill*, Siegel V. Ed. Advances in Polar Ecology**:** 21-100.

Silva T.A.M., Bigg G.R. & Nicholls K.W. 2006. Contribution of giant icebergs to the Southern Ocean freshwater flux. *Journal of Geophysical Research*, **111**: C03004.

Sokolov S. & Rintoul S.R. 2009. Circumpolar structure and distribution of the Antarctic Circumpolar Current fronts: 1. Mean circumpolar paths. *Journal of Geophysical Research*, **114**: C11018.

Spence P., Holmes R.M., Hogg A.M., Griffies S.M., Stewart K.D. & England M.H. 2017. Localized rapid warming of West Antarctic subsurface waters by remote winds. *Nature Climate Change*, **7** (8): 595-603.

Stammerjohn S.E., Martinson D.G., Smith R.C. & Iannuzzi R.A. 2008a. Sea ice in the western Antarctic Peninsula region: Spatio-temporal variability from ecological and climate change perspectives. *Deep-Sea Research Part II: Topical Studies in Oceanography*, **55** (18-19): 2041-2058.

Stammerjohn S.E., Martinson D.G., Smith R.C., Yuan X. & Rind D. 2008b. Trends in Antarctic annual sea ice retreat and advance and their relation to El Niño–Southern Oscillation and Southern Annular Mode variability. *Journal of Geophysical Research*, **113** (C3): C03S90.

Stone E.J., Capron E., Lunt D.J., Payne A.J., Singarayer J.S., Valdes P.J. & Wolff E.W. 2016. Impact of meltwater on high-latitude early Last Interglacial climate. *Climate of the Past*, **12** (9): 1919-1932.

Tournadre J., Bouhier N., Girard-Ardhuin F. & Rémy F. 2016. Antarctic icebergs distributions 1992–2014. *Journal of Geophysical Research: Oceans*, **121** (1): 327-349.

Trathan P.N., Brandon M.A., Murphy E.J. & Thorpe S.E. 2000. Transport and structure within the Antarctic Circumpolar Current to the north of South Georgia. *Geophysical Research Letters*, **27** (12): 1727-1730.

Turney C.S.M., Jones R., McKay N.P., van Sebille E., Thomas Z.A., Hillenbrand C.-D. & Fogwill C.J. 2020. A global mean sea-surface temperature dataset for the Last Interglacial (129-116 kyr) and contribution of thermal expansion to sea-level change. *Earth System Science Data Discussions*, **12** (4): 3341-3356.

Turney C.S.M. & Jones R.T. 2010. Does the Agulhas Current amplify global temperatures during super-interglacials? *Journal of Quaternary Science*, **25** (6): 839-843.

Vaughan D.G., Comiso J.C., Allison I., Carrasco J., Kaser G., Kwok R., Mote P., Murray T., Paul F., Ren J., Rignot E., Solomina O., Steffen K. & Zhang T. 2013. Observations: Cryosphere. In: *Climate Change 2013: The Physical Science Basis, Contribution of Working Group I to the Fifth Assessment Report of the Intergovernmental Panel on Climate Change.*, Stocker T.F., Qin D., Plattner G.-K. et al. Eds. Cambridge University Press, Cambridge, United Kingdom and New York, NY, USA.**:** 317-382.

Vernet M., Geibert W., Hoppema M., Brown P.J., Haas C., Hellmer H.H., Jokat W., Jullion L., Mazloff M., Bakker D.C.E., Brearley J.A., Croot P., Hattermann T., Hauck J., Hillenbrand C.D., Hoppe C.J.M., Huhn O., Koch B.P., Lechtenfeld O.J., Meredith M.P., Naveira Garabato A.C., Nöthig E.M., Peeken I., Rutgers van der Loeff M.M., Schmidtko S., Schröder M., Strass V.H., Torres-Valdés S. & Verdy A. 2019. The Weddell Gyre, Southern Ocean: Present Knowledge and Future Challenges. *Reviews of Geophysics*, **57** (3): 623-708.

Walter J.I., Box J.E., Tulaczyk S., Brodsky E.E., Howat I.M., Ahn Y. & Brown A. 2012. Oceanic mechanical forcing of a marine-terminating Greenland glacier. *Annals of Glaciology*, **53** (60): 181-192.

Wang Z. 2013. On the response of Southern Hemisphere subpolar gyres to climate change in coupled climate models. *Journal of Geophysical Research: Oceans*, **118** (3): 1070-1086.

Weber M.E., Kuhn G., Sprenk D., Rolf C., Ohlwein C. & Ricken W. 2012. Dust transport from Patagonia to Antarctica – A new stratigraphic approach from the Scotia Sea and its implications for the last glacial cycle. *Quaternary Science Reviews*, **36**: 177-188.

Weber M.E., Niessen F., Kuhn G. & Wiedicke M. 1997. Calibration and application of marine sedimentary physical properties using a multi-sensor core logger. *Marine Geology*, **136**: 151-172.

Williams T.J. 2018. Investigating the circulation of Southern Ocean deep water masses over the last 1.5 million years by geochemical fingerprinting of marine sediments. PhD thesis: *Department of Earth Sciences, University of Cambridge.*

Zielinski U. & Gersonde R. 1997. Diatom distribution in Southern Ocean surface sediments (Atlantic sector): Implications for paleoenvironmental reconstructions. *Palaeogeography, Palaeoclimatology, Palaeoecology*, **129**: 213-250.